Canadian Journal of Chemistry

Article

Weak and strong π interactions between two monomers—assessed with local vibrational mode theory

Wenli Zou[a,b], **Marek Freindorf**[a], **Vytor Oliveira**[c], **Yunwen Tao**[a], **and Elfi Kraka**[a]

[a]Computational and Theoretical Chemistry Group (CATCO), Department of Chemistry, Southern Methodist University, 3215 Daniel Ave, Dallas, TX 75275-0314, USA; [b]Institute of Modern Physics, Northwest University Xi'an, Shaanxi, 710127, China; [c]Departamento de Quimica Instituto Tecnologico de Aeronautica (ITA), Sao Jose dos Campos, Sao Paulo, SP 12228-900, Brazil

Corresponding author: **Elfi Kraka** (email: ekraka@gmail.com)

Can. J. Chem. Downloaded from cdnsciencepub.com by University of Alberta on 09/01/23
For personal use only.

Abstract

We introduce in this work a unique parameter for the quantitative assessment of the intrinsic strength of the π interaction between two monomers forming a complex. The new parameter is a local intermonomer stretching force constant, based on the local mode theory, originally developed by Konkoli and Cremer, and derived from the set of nine possible intermonomer normal vibrational modes. The new local force constant was applied to a diverse set of more than 70 molecular complexes, which was divided into four groups. Group 1 includes atoms, ions, and small molecules interacting with benzene and substituted benzenes. Group 2 includes transition metal hydrides and oxides interacting with benzene while Group 3 involves ferrocenes, chromocenes, and titanium sandwich compounds. Group 4 presents an extension to oxygen π–hole interactions in comparison with in-plane hydrogen bonding. We found that the strength of the π interactions in these diverse molecular complexes can vary from weak interactions with predominantly electrostatic character, found, e.g., for argon–benzene complexes, to strong interactions with a substantial covalent nature, found, e.g., for ferrocenes; all being seamlessly described and compared with the new intermonomer local mode force constant, which also outperforms other descriptors such as an averaged force constant or a force constant guided by the electron density bond paths. We hope that our findings will inspire the community to apply the new parameter also to other intermonomer π interactions, enriching in this way the broad field of organometallic chemistry with a new efficient assessment tool.

Key words: local mode analysis, intermonomer force constant, sandwich complexes, vibrational spectroscopy

Introduction

Noncovalent interactions between monomers leading to complex formation is the topic of many experimental and computational investigations, because of the vital role they play in the structure and properties of chemical and biological systems and materials,[1–13] as well as their chemical reactions.[14] Among the diverse noncovalent interactions present between molecules, systems with π interactions have recently attracted a lot of attention[3,15] including cation–π,[16] anion–π,[17–22] CH–π,[23–27] BH–π,[28,29] lone pair–π,[30–33] and π–π interactions of various forms.[34,35] In addition, there are also strong, mostly covalent π interactions as found in particular in metal–π sandwich compounds.[36–39] In particular, metallocenes (i.e., two cyclopentadienyl (Cp) anions bound to a metal center) belong to an important class of complexes in organometallic chemistry, which have attracted a similar attention as their noncovalent counterparts. Since the discovery of ferrocene[40,41] they have been a topic of many experimental and computational investigations, because of their rich potential as catalysts[42–48] as new materials in porous structures,[49,50] molecular magnets,[51] or as qubits in quantum computing,[52] as well as their potential use for medicinal chemistry.[53,54] Recently, metallocenes with a tilted Cp framework caused by a carbon-based bridge, the so-called *ansa-metallocenes* [55] have attracted a lot of attention, in particular Ti, Zr, and Hf metallocenes[56,57] as well as sandwich complexes involving lanthanides and actinides,[58–64] both enriching the organometallic repertoire.

The strength of noncovalent π interactions is usually measured by the complex binding energy ΔE_B or the complex interaction energy ΔE_I. ΔE_B is defined as the difference between the energy of the complex and the energy of the isolated monomers in their minimum configuration, which can be both measured or calculated,[65–67] whereas ΔE_I is a theoretical measure, defined as the difference between the energy of the complex and the energy of the isolated monomers in the geometry of the complex.[68–73] As such, ΔE_B provides a more realistic measure of the complex stability as it includes the geometry and electron density reorganization of the monomers upon complex formation. It is often assumed that ΔE_B or ΔE_I provide a measure of the intrinsic bond strength of the noncovalent interaction in question. However, this might not even be true in a qualitative sense, as ΔE_B or ΔE_I are cumulative properties, i.e., they are the

Can. J. Chem. Downloaded from cdnsciencepub.com by University of Alberta on 09/01/23
For personal use only.

sum of all interactions between the monomers including, e.g., long-range electrostatic interactions, that may even involve more remote atoms of the monomers.[74] Therefore, it is difficult to single out a specific interaction between atoms or groups of the monomers. Energy decomposition schemes are a popular computational approach leading to qualitative, model-dependent results.[75–80] The strength of the π interactions in metal–sandwich complexes is often determined via molecular orbital (MO) analyses and/or ligand field considerations, again leading to more qualitative results.[81,82] In this situation, vibrational spectroscopy provides an excellent alternative for the assessment of the interactions between two monomers forming a complex.[83] In particular, the intermonomer normal vibrations[84–90] offer a unique platform for a spectroscopic measure of the intrinsic strength of the intermonomer interaction in π complexes when combined with the local vibrational mode theory originally developed by Konkoli and Cremer.[91–95] We derived in this work a unique local mode stretching force constant for the quantitative description of these intermonomer π interactions, a necessary prerequisite for a detailed understanding and assessment of how these interactions influence molecular properties and reactivity; an important tool, which so far is still missing. The new local intermonomer force constant was then applied to a test set of complexes shown in Fig. 1 covering four different scenarios; Group 1: π interaction between benzene and an atom/molecule containing main group elements including benzene–A and benzene–AH_n complexes, benzene–C_2H_2 and benzene–C_2H_4 complexes[96–98] (complexes **1–38**); Group 2: π interaction between benzene and transition metal hydrides/oxides (complexes **39–49**); Group 3: sandwich complexes including ferrocenes, Cr, and Ti complexes, and Cr reference compounds[99–102] (complexes **50–67**); Group 4: Simplified model of the gallic acid dimer complex **68** probing the recently suggested oxygen–π hole interactions occurring in addition to in-plane hydrogen bonding, when exposed to ether **69**, ketone **70**, or fluoro-substituted ether **71**,[103] as well as acetic and formic acid dimers **72** and **73** and the water dimer **74** as references for the in-plane hydrogen bonds. It has to be noted that in this work we refer to π interaction in the traditionally sense, i.e., being defined as an interaction that involves an electron-rich π system, without a specific discussion of the π symmetry of specific orbitals.

The manuscript is structured in the following way: First, we summarize the essential features of local vibrational mode theory and its connection to Wilson's GF normal mode analysis.[84–90] For a comprehensive review of the local vibrational mode theory the reader may refer to reference.[104] Then we will derive type and number of intermonomer normal vibrational modes in a dimer complex, their connection to the corresponding local vibrational modes, and define a suited local intermonomer force constant measuring the strength of the intermonomer interaction for the π complexes studied in this work, which have at least one ring monomer. A discussion of defining the interaction strength via averaged force constants or force constants guided by electron density bond paths (BPs) follows pointing out the weaknesses of these approaches as demonstrated for the Ar–C_{18} complex. After the computational details, we present the results for the complexes shown in Fig. 1, assessing in particular the performance of our new intermonomer local force constant. Conclusions and outlook are given in the last part.

Methodology

Normal mode analysis, Wilson GF formalism

In eq. 1, the Wilson equation of vibrational spectroscopy for a vibrating systems with N atoms is given:[84–90]

$$\mathbf{F}^x\tilde{\mathbf{L}} = \mathbf{M}\tilde{\mathbf{L}}\mathbf{\Lambda} \quad (1)$$

where $\mathbf{F}^x$ is the force constant matrix expressed in Cartesian coordinates x_i ($i = 1, ..., 3N$). $\mathbf{M}$ is the diagonal mass matrix containing the atomic mass for each atom three times to account for the motion in x, y, and z directions, and matrix $\tilde{\mathbf{L}}$ collects the vibrational eigenvectors $\tilde{\mathbf{l}}_\mu$ in its columns ($\mu = 1, ..., N_{vib}$). The number of vibrational modes N_{vib} equals $3N - N_{tr}$ with the translational and rotational modes N_{tr} being 5 for linear and 6 for nonlinear molecules. $\mathbf{\Lambda}$ is a diagonal matrix with the eigenvalues λ_μ, which leads to the (harmonic) vibrational frequencies ω_μ according to $\lambda_\mu = 4\pi^2c^2\omega_\mu^2$. The tilde symbol indicates mass weighting. The normal mode eigenvectors and eigenvalues are obtained by diagonalizing the force constant matrix $\mathbf{F}^x$ defined in eq. 1 according to $\tilde{\mathbf{L}}^\dagger\mathbf{F}^x\tilde{\mathbf{L}} = \mathbf{\Lambda}$ with the normalization condition $\tilde{\mathbf{L}}^\dagger\mathbf{M}\tilde{\mathbf{L}} = \mathbf{I}$.

Usually, the normal mode vectors $\tilde{\mathbf{l}}_\mu$ are renormalized according to $\mathbf{L} = \tilde{\mathbf{L}}\left(\mathbf{M}^R\right)^{1/2}$, where the elements of the mass matrix $\mathbf{M}^R$ are given by $m_\mu^R = \left(\tilde{\mathbf{l}}_\mu^\dagger\tilde{\mathbf{l}}_\mu\right)^{-1}$ and represent the reduced mass of mode μ.

Equation 1 can be written in different ways.[84,85,89] For example, without mass-weighting eq. 1 takes the form

$$\mathbf{F}^x\mathbf{L} = \mathbf{ML}\mathbf{\Lambda} \quad (2)$$

leading to the diagonal normal force constant matrix $\mathbf{K}$, and the reduced mass matrix $\mathbf{M}^R$ in normal coordinates $\mathbf{Q}$, respectively.

$$\mathbf{L}^\dagger\mathbf{F}^x\mathbf{L} = \mathbf{K} \quad (3)$$

$$\mathbf{L}^\dagger\mathbf{ML} = \mathbf{M}^R \quad (4)$$

The dimension of matrices $\mathbf{K}$ and $\mathbf{M}^R$ is $N_{vib} \times N_{vib}$.

One can also express the molecular geometry in terms of internal coordinates $\mathbf{q}$ rather than Cartesian coordinates $\mathbf{x}$, and by this the Wilson equation adopts a new form:[84]

$$\mathbf{F}^q\mathbf{D} = \mathbf{G}^{-1}\mathbf{D}\mathbf{\Lambda} \quad (5)$$

where $\mathbf{D}$ collects the normal mode vectors $\mathbf{d}_\mu$ ($\mu = 1, ..., N_{vib}$) columnwise, and the Wilson matrix $\mathbf{G}$, which is defined as

$$\mathbf{G} = \mathbf{BM}^{-1}\mathbf{B}^\dagger \quad (6)$$

represents the kinetic energy in terms of internal coordinates. The elements of the rectangular $\mathbf{B}$ matrix in eq. 6 are defined by the partial derivatives of internal coordinates q_n ($n = 1, 2, 3, ..., N_{vib}$) with regard to Cartesian

Fig. 1. Complexes investigated in this work. Intermonomer distances (Å) in green, corresponding local mode forces constants (mDyn/Å) in blue, and local mode frequencies (cm^{-1}) in red. For a description of model chemistries used, see computational details.

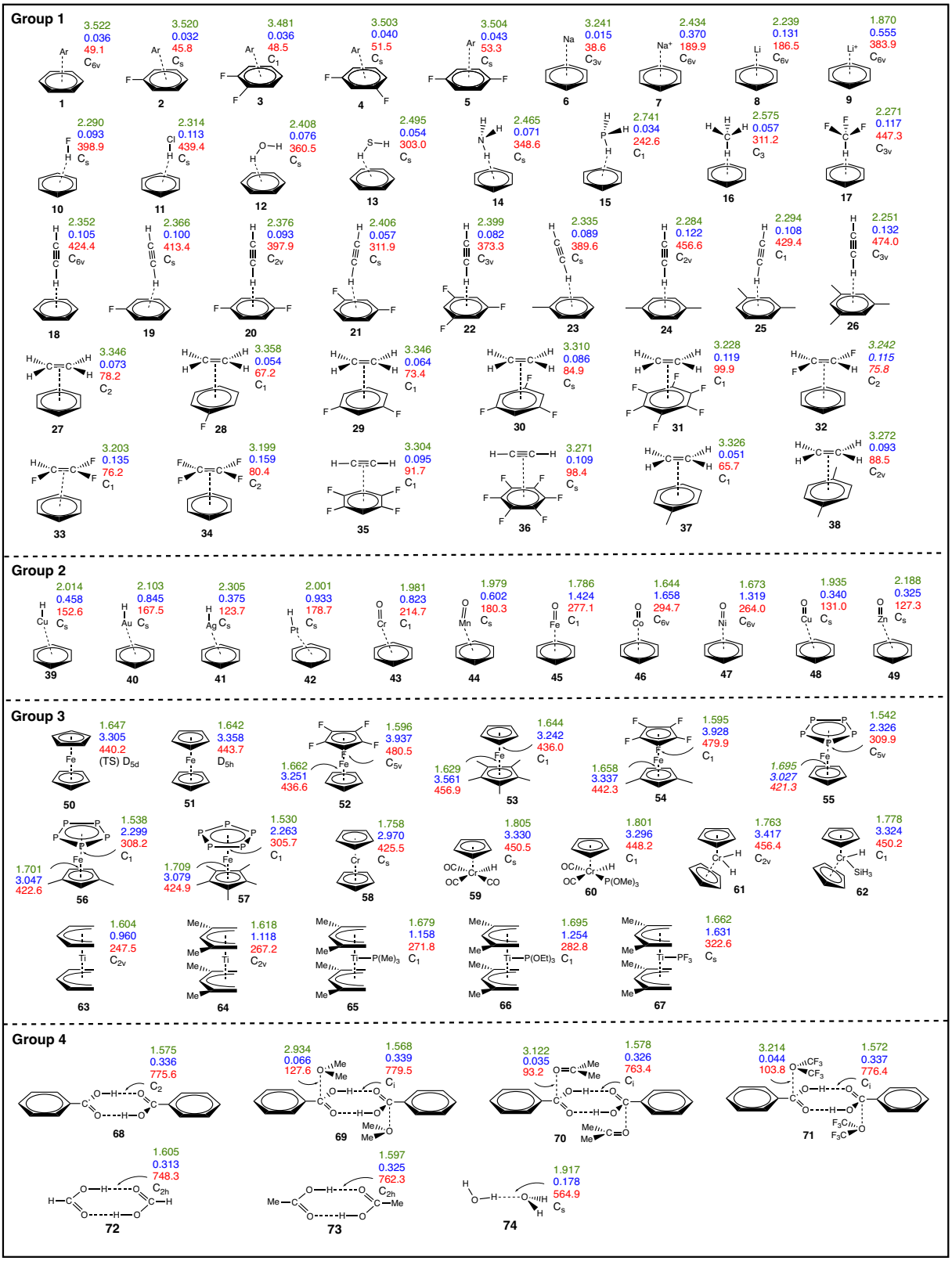

Can. J. Chem. Downloaded from cdnsciencepub.com by University of Alberta on 09/01/23
For personal use only.

Can. J. Chem. Downloaded from cdnsciencepub.com by University of Alberta on 09/01/23
For personal use only.

coordinates x_i ($i = 1, 2, 3, ..., 3N$),

$$\mathbf{B}_n = \frac{\delta q_n(\mathbf{x})}{\delta x_i} \quad (7)$$

It is important to note that the **B** matrix plays a central role for the Wilson equation of spectroscopy, namely connecting different sets of coordinates (internal, symmetry, curvilinear, etc.)[105–107] or Cremer–Pople ring puckering coordinates,[108] with the Cartesian coordinates.[84] Therefore, whenever a new set of coordinates is introduced, the first step is to derive the appropriate **B** matrix, as demonstrated below for the definition of intermonomer modes.

Diagonalization of eq. 5 leads to

$$\mathbf{D}^{\dagger}\mathbf{F}^{q}\mathbf{D} = \mathbf{K} \quad (8)$$

Equations 2 and 5 are connected by the following equations,[84]

$$\mathbf{F}^{\mathbf{q}} = \mathbf{C}^{\dagger}\mathbf{F}^{\mathbf{x}}\mathbf{C} \quad (9)$$

$$\mathbf{D} = \mathbf{BL} \quad (10)$$

Matrix **C** is the pseudoinverse of the **B** matrix defined by

$$\mathbf{C} = \mathbf{W}\mathbf{B}^{\dagger}\left(\mathbf{B}\ \mathbf{W}\ \mathbf{B}^{\dagger}\right)^{-1} \quad (11)$$

where **W** is an arbitrary nonsingular $3N \times 3N$ square matrix. At a stationary point (i.e., the energy gradient is a zero vector), the N_{tr} translational and rotational eigenvectors are decoupled from the N_{vib} vibrational eigenvectors, and therefore **W** does not affect the results.[109] For reasons of simplicity, one often uses $\mathbf{W} = \mathbf{I}_{3N}$ (usually for the geometry optimization procedure in internal coordinates) or $\mathbf{W} = \mathbf{M}^{-1}$. Using the latter definition, which is more physically sound[110] (see also references 11–13 therein), this leads to

$$\mathbf{C} = \mathbf{M}^{-1}\mathbf{B}^{\dagger}\mathbf{G}^{-1} \quad (12)$$

and

$$\mathbf{BC} = \mathbf{I}_{N_{vib}} \quad (13)$$

It should be noted that $\mathbf{CB} \neq \mathbf{I}_{3N}$ since **B** is spanned in an N_{vib}-dimensional vibrational space.

The transformation to normal coordinates **Q** leading to the diagonal force constant matrix **K** and normal mode vectors $\mathbf{d}_{\mu}$ (see eq. 8) is a standard procedure in modern quantum chemistry packages calculating vibrational frequencies, providing access to important electronic structure information of a molecule and the motion of its atoms for each of the N_{vib} vibrations.[111–113] In addition, modern experimental vibrational spectroscopy provides vibrational frequencies ranging from near- to far-infrared regions, thanks to rapidly advancing technologies.[114–120] Therefore, vibrational frequencies and related force constants have become a popular measure of bond strength. However, caveat is appropriate. As already pointed out by Wilson in 1941,[121] normal coordinates **Q** are generally a linear combination of internal coordinates **q** or Cartesian coordinates **x**

$$Q_{\mu} = \sum_{j}^{N_{vib}} \left(\tilde{\mathbf{D}}^{\dagger}\mathbf{G}^{-1}\right)_{\mu j} q_j \quad (14)$$

$$Q_{\mu} = \sum_{j}^{3N} \left(\tilde{\mathbf{D}}^{\dagger}\mathbf{G}^{-1}\mathbf{B}\right)_{\mu j} x_j \quad (15)$$

leading to normal vibrational modes that are generally delocalized over the molecule and in this way limiting the use of normal mode frequencies and normal mode force constants as bond strength measure. For this purpose, local vibrational modes and related local mode frequencies and force constants are needed, which are described in the following section.

Local vibrational mode analysis

The local vibrational mode analysis (LMA), both theory and application has been amply described in previous work,[91–95,104,109] and therefore we present in the following only some of the key features. In 1998, Konkoli and Cremer[91,92] derived for the first time local vibrational modes directly from normal vibrational modes by solving the mass-decoupled Euler–Lagrange equations, i.e., by solving the local equivalent of the Wilson equation for vibrational spectroscopy. They developed the leading parameter principle[91,92] which states that for any internal, symmetry, curvilinear, etc. coordinate a local mode $\mathbf{a}_n$ can be defined. $\mathbf{a}_n$ is independent of all other internal coordinates used to describe the geometry of a molecule, which means that it is also independent of using redundant or nonredundant coordinate sets. The local mode vector $\mathbf{a}_n$ associated with the n-th internal coordinate q_n is defined as[91,92]

$$\mathbf{a}_n = \frac{\mathbf{K}^{-1}\mathbf{d}_n^{\dagger}}{\mathbf{d}_n\mathbf{K}^{-1}\mathbf{d}_n^{\dagger}} \quad (16)$$

where the local mode $\mathbf{a}_n$ is expressed in terms of normal coordinates **Q** and $\mathbf{d}_n$ is the n-th row vector of the **D** matrix defined in eq. 10.

Equation 16 reveals that only matrices **K** and **D** are needed to determine $\mathbf{a}_n$, i.e., once the normal analysis is completed, a following local mode analysis is straightforward.[91,92]

To each local mode $\mathbf{a}_n$ local mode properties can be assigned. The *local mode force constant* k_n^a of mode n (superscript a denotes an adiabatically relaxed, i.e., local mode) is obtained via eq. 17:

$$k_n^a = \mathbf{a}_n^{\dagger}\mathbf{K}\mathbf{a}_n = \left(\mathbf{d}_n\mathbf{K}^{-1}\mathbf{d}_n^{\dagger}\right)^{-1} \quad (17)$$

It is noteworthy that local mode force constants, contrary to normal mode force constants, have the advantage of being independent of the choice of the coordinates used to describe the molecule in question.[91,95] In recent work, Zou and co-workers proved that the compliance constants Γ_{nn} of Decius[122] are simply the reciprocal of the local mode force constants: $k_n^a = 1/\Gamma_{nn}$.[109]

The *local mode mass* m_n^a of mode n is given by

$$m_n^a = 1/G_{n,n} = \left(\mathbf{b}_n\mathbf{M}^{-1}\mathbf{b}_n^{\dagger}\right)^{-1} \quad (18)$$

where $G_{n,n}$ is the n-th diagonal element of the Wilson **G** matrix. For a chemical bond A–B, eq. 18 leads to $M_A M_B/(M_A + M_B)$, which has the same form as the reduced mass of diatomic molecules.

Can. J. Chem. Downloaded from cdnsciencepub.com by University of Alberta on 09/01/23
For personal use only.

Local mode force constant and mass are needed to determine the *local mode frequency* ω_n^a

$$(19)\quad \left(\omega_n^a\right)^2 = \frac{1}{4\pi^2 c^2} k_n^a G_{nn}$$

Apart from these properties, it is straightforward to determine the local mode infrared intensity.[123]

Local and normal vibrational modes are connected via an adiabatic connection scheme,[109] which has opened the avenue to a new way of analyzing vibrational spectra—the composition of normal mode (CNM) analysis.[104] Normal vibrational modes can be decomposed into local mode components for a complete, nonredundant set of N_{vib} local modes;[93,95] a new way of decoding the rich information contained in a vibrational spectrum.[104,124–126] For this purpose, Konkoli and Cremer introduced an amplitude $\mathcal{A}$ which provides a measure for the contribution of the local vibrational modes to each normal vibrational mode. They defined $\mathcal{A}$ as a function of normal mode $\mathbf{l}_\mu$ and local mode $\mathbf{a}_n$

$$(20)\quad \mathcal{A}_{n\mu} = \frac{\left(\mathbf{I}_\mu, \mathbf{a}_n\right)^2}{\left(\mathbf{a}_n, \mathbf{a}_n\right)\left(\mathbf{I}_\mu, \mathbf{I}_\mu\right)}$$

The denominator in eq. 20 normalizes $\mathcal{A}$ so that its value lies between 0 and 1. The matrix (**a**,**b**) in eq. 20 is expressed as

$$(21)\quad (\mathbf{a}, \mathbf{b}) = \sum_{i,j} a_i f_{ij} b_j$$

where a ∈ [$\mathbf{I}_\mu$, $\mathbf{a}_n$], b ∈ [$\mathbf{I}_\mu$, $\mathbf{a}_n$], and f_{ij} are elements of the force constant matrix $\mathbf{F}^x$ expressed in Cartesian coordinates. Once $\mathcal{A}$ is defined, the percentage of the local mode contributions to a certain normal mode can be compared by

$$(22)\quad \mathcal{A}_{n\mu}^{\%} x; = \frac{\mathcal{A}_{n\mu}}{\sum_m \mathcal{A}_{m\mu}} 100$$

where $\sum_m \mathcal{A}_{m\mu}$ represents the sum of all amplitudes related to the normal mode in question.

In this work, we used CNM to assess the physical relevance of the new local intermonomer mode as descriptor of the interaction between the two monomers, as discussed below.

In summary, LMA has advanced over the past years as a powerful bond strength descriptor accounting for both covalent bonds and noncovalent interactions stretching from hydrogen bonds, halogen bonds to tetrel bonds and π–hole interactions. Some recent examples are presented in references.[31,127,128] Different molecular environments were considered such as systems in solution[129] or in proteins.[130] Another focus has been metal–ligand bonding which led to a new metal ligand electronic parameter replacing, e.g., the Tolman electronic parameter.[131,132] The local mode analysis of periodic systems and crystals was recently added to the repertoire.[133,134] For a comprehensive discussion of LMA applications the reader is referred to reference[104] and references therein. In the following section, the focus is deriving a set of nonredundant local intermonomer modes, with the emphasis on defining a physically sound local intermonomer mode being directly connected to the strength of the interaction between the two monomers. In this way covalent π bonds and weak π interactions can for the first time be seamlessly compared leading to new insights into the strategic functionalization of these interactions for the design of new materials.

Intermolecular modes in a dimeric system

For two isolated polyatomic monomers A and B (for the general case we assume that A and B are nonlinear with the number of atoms being N_A for A and N_B for B, respectively), one can choose a set of nonredundant $N_{vib}^A = 3N_A - 6$ local modes for monomer A and a set of nonredundant $N_{vib}^B = 3N_B - 6$ local modes for monomer B, respectively. When the two monomers with a total of 12 translations and rotations combine to form a complex AB, 6 of these translations and rotations transform into intermolecular vibrations describing stretching, bending, and torsion of the monomers relative to each other,[84] and therefore the $N_{vib}^{AB} = N_{vib}^A + N_{vib}^B + 6$ modes compose a new set of nonredundant local modes for the dimer. To define these intermolecular vibrations in a unique way, both monomers have to be rotated into a uniquely defined standard orientation, which is in general not possible. However, if one monomer, (in this work always monomer B) is a ring, the arbitrary rectangular coordinate system can be rotated into the standard orientation, which is uniquely defined by the Cremer–Pople mean ring plane[108] of the ring atoms in monomer B.

First, each atom in monomer B has to be rotated into the standard orientation by a 3 × 3 rotation matrix **r** (see reference[108]), i.e., the coordinate system is transformed from the initial *xyz* to the standard *x′y′z′*. The atoms in monomer A are then also rotated by **r**, bringing the dimer AB into this standard. As shown in Fig. 2, O_A is the geometric center of the rotated monomer A, O_B and *x′y′z′* define the standard orientation of monomer B determined by the mean plane,[108] respectively, and *x″y″z″* is the shifted coordinate system *x′y′z′* from O_B to O_A. Using the Ekart–Sayvetz conditions,[135] three mass-irrelevant (that is, all the atomic masses are 1) translation modes in the *x′*, *y′*, and *z′* directions and three mass-irrelevant rotation modes around the *x′*, *y′*, and *z′* axes can be defined for monomer B, i.e., $\mathbf{T}_B^x$, $\mathbf{T}_B^y$, $\mathbf{T}_B^z$, $\mathbf{R}_B^x$, $\mathbf{R}_B^y$, and $\mathbf{R}_B^z$. In a similar way, column arrays $\mathbf{T}_A^x$, $\mathbf{T}_A^y$, $\mathbf{T}_A^z$, $\mathbf{R}_A^x$, $\mathbf{R}_A^y$, and $\mathbf{R}_A^z$ can be obtained for monomer A in the *x″y″z″* coordinate system.

These monomer modes define nine intermonomer modes applying the Wilson B-matrix formalism.[84] If the atoms in A are given first, Wilson's B-matrices (notice that they are row arrays) of nine intermolecular local modes can be calculated by

$$(23)\quad \mathbf{b}^\dagger(S_X) = \left(\frac{1}{\sqrt{N_A}}\mathbf{T}_A^X \;\; \frac{-1}{\sqrt{N_B}}\mathbf{T}_B^X\right),\quad \mathbf{b}^\dagger(R_X) = \left(\frac{1}{\sqrt{N_A}}\mathbf{R}_A^X \;\; \frac{1}{\sqrt{N_B}}\mathbf{R}_B^X\right),$$
$$\mathbf{b}^\dagger(A_X) = \left(\frac{1}{\sqrt{N_A}}\mathbf{R}_A^X \;\; \frac{-1}{\sqrt{N_B}}\mathbf{R}_B^X\right)$$

where *S*, *R*, and *A* represent intermolecular stretching, rotation, and antirotation modes, respectively; *X* = *x*, *y*, or *z*, (as shown in Fig. 2) and the factor $1/\sqrt{N_A}$ or $1/\sqrt{N_B}$ denotes that the deformation amplitude of each monomer is set to 1. The B-matrices in eq. 23 then have to be rotated back to the initial orientation by **r**.

Fig. 2. Definition of the interaction between an atom/molecule A and a benzene ring B. O_A is the geometric center of the rotated monomer A, O_B and $x'y'z'$ define the standard orientation of ring B determined by the mean plane.[108] $x''y''z''$ is the shifted coordinate system $x'y'z'$ from O_B to O_A. The framed **Sz** motion is used in this work to define the interaction between A and B.

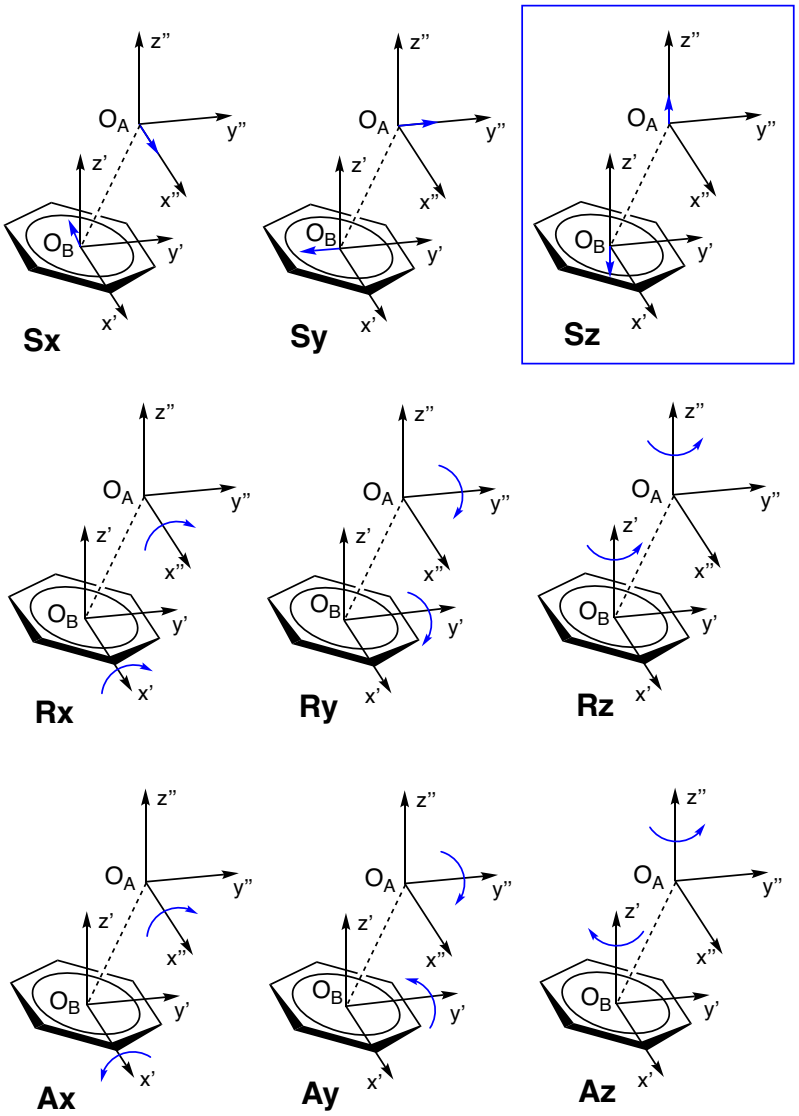

Out of these nine intermonomer modes, we preferentially chose the three intermolecular stretching modes S_x, S_y, S_z and the three intermolecular rotational modes R_x, R_y, R_z[124] to construct a set of six nonredundant intermonomer coordinates. There are a few exceptions to be mentioned.

- A is an atom ($N_A = 1$ and $N_{vib}^{AB} = N_{vib}^{B} + 3$). In this case, there are no rotations $\mathbf{R}_A^X$ and only the three intermolecular stretching modes S_X are relevant.
- A is linear ($N_A \geqslant 2$), and its molecular axis is parallel to the X'' axis. In this case, the $\mathbf{R}_A^X$ rotation does not exist and only five intermolecular modes remain, e.g., S_x, S_y, S_z, R_x, R_y.
- A is nonlinear ($N_A \geqslant 3$) but X' and X'' are collinear. In this case, the R_X mode becomes a pure rotational mode of the AB dimer and does not have to be considered.

In summary, among the three intermolecular stretching modes S_x, S_y, S_z, the two modes S_x and S_y describe sliding of A along the mean plane of the ring system B in two orthogonal directions, whereas S_z corresponds to the genuine stretching between the monomers A and B, thus reflecting the interaction between the two monomers. Therefore, the focus in this work is on the S_z mode, whereas the purpose of S_x and S_y (as well as the other intermolecular modes R_X and A_X) is to construct a nonredundant deformation space.

Since the intermonomer local modes of a dimer system are linear combinations of translational or rotational modes of two monomers, they may be not free from the contamination of translational or rotational modes of the dimer system, and therefore it is necessary to project out residual translations and rotations from the local force constants. For this purpose the n-th vector $\mathbf{b}_n$ of the B matrix defined

Can. J. Chem. Downloaded from cdnsciencepub.com by University of Alberta on 09/01/23
For personal use only.

Can. J. Chem. Downloaded from cdnsciencepub.com by University of Alberta on 09/01/23
For personal use only.

in eq. 7 has to be calculated according to the extended formula,

$$\bar{\mathbf{d}}_n = \mathbf{b}_n \bar{\mathbf{L}} \quad (24)$$

leading to the projected force constant $k_n^{a,p}$ given by

$$k_n^{a,p} = \frac{\mathbf{d}_n \mathbf{d}_n^\dagger}{\bar{\mathbf{d}}_n \bar{\mathbf{d}}_n^\dagger} k_n^a \quad (25)$$

where the dimension of $\bar{\mathbf{L}}$ is $3N \times 3N$, i.e., in addition to the N_{vib} vibrations the N_{tr} translational and rotational are included. In Table 1, the local mode force constants and local mode frequencies between monomers A = Ar (**1**), HF (**10**), H_2O (**12**), NH_3 (**14**), CH_4 (**16**), and B = C_6H_6 (see Fig. 1) as well as for the perpendicular and parallel benzene dimer $(C_6H_6)_2$ are collected, showing the influence of the projection on the three stretching modes S_x, S_y, and S_z. As obvious from the data in Table 1 local mode force constants $k_a(S_x)$ and $k_a(S_y)$ as well as the corresponding frequencies $\omega_a(S_x)$ and $\omega_a(S_y)$ are more affected by the projection than those defined for S_z mode. In particular, the last three entries of Table 1, **1** calculated with the long range-corrected[136] version of the B97 functional plus Grimme's D3BJ dispersion schemes[137] (LC-B97D3) with the def2-TZVPP basis set and the density fitting approximation[138] and the parallel and perpendicular benzene dimers calculated with a B2PLYPD/AVTZ model chemistry demonstrate the strong influence of the density functional used on this projection. For **1** the $k_a(S_x)$ and $k_a(S_y)$ force constants are 0.415 mDyn/Å before and 0.066 mDyn/Å after the translational and rotational contributions are projected out, which has to be considered when describing these weak interactions with a density functional model chemistry.

Other choices of intermonomer force constants

Averaged local force constant

One could think of calculating the local modes for all A– or O_A–carbon ring interactions and averaging over the corresponding local mode force constants. However, such an averaged local force constant leads to redundancies, because there are just six intermolecular vibrational modes in total between the interacting monomers, as discussed above. In addition, such an approach can lead to an erroneous assessment of the strength of the atom/molecule–ring interaction as shown in the following for the Ar–C_{18} complex.

The cyclo[18]carbon (C_{18}) monomer was experimentally detected in 2019.[142] It has a planar cyclopolyene minimum structure with alternating weaker and stronger CC bonds with D_{9h} symmetry and a cumulene transition structure with identical CC bonds with D_{18h} symmetry. In a recent work, we analyzed the C_{18} potential energy surface and its pseudorotation path in the space of deformation coordinates at the M06-2X/def2-TZVPP level of theory.[143] The same model chemistry was adopted in this work for the investigation of the Ar–C_{18} complex. We found that the Ar–C_{18} complex adopts a planar minimum structure with D_{9h} symmetry with alternating weaker and stronger CC bonds in the case of the C_{18} monomer and the Ar atom being located in the ring center, as is sketched in Fig. 3.

The subsequent CNM analysis, shown in Fig. 4 reveals the shortcomings of an ansatz based an averaged local (ArC) force constant as interaction strength descriptor. Pictures of selected Ar–C_{18} normal mode vibrations (Fig. S1) as well as the corresponding movies (Table S1) showing the movement of the atoms during these normal mode vibrations can be found in the Supporting Information. The lowest $1a_2''$ normal mode (Fig. 4*a*, yellow color, normal mode frequency of 14 cm^{-1}) is 100% composed of the S_z mode, describing the out of plane motion of the Ar atom. The two degenerate $1e_1'$ normal modes with a frequency of 55 cm^{-1} are each composed of 97% S_y and S_x, respectively, describing the sliding of the Ar atom in y and x directions. As a consequence of this sliding motion the ArC distance changes, clearly revealing that an averaged local (ArC) force constant is not a suitable descriptor for the strength of the interaction between the Ar atom and that the S_z coordinate is the most appropriate choice for description of the van der Waals interaction between Ar and the cyclo[18]carbon ring.

The CNM analysis of the Ar–C_{18} complex (Fig. 4) also discloses a number of additional interesting features with regard to in plane and out of plane puckering of the C18 ring based on the Cremer–Pople puckering coordinates.[105,108,143] The CNM analysis of this system requires a set of 51 nonredundant local coordinates, which is made of 15 out of plane ring puckering coordinates (label Q in Fig. 4) and 32 in plane ring deformation coordinates (label T in Fig. 4), in addition to coordinates τ_9 (Tau9), coordinate (R) describing overall ring deformation and ring breathing, and the three coordinates S_z, S_x, and S_y describing in plane and out of plane motion of the Ar atom relative to the cyclo[18]carbon ring. Further details of the puckering and deformation analysis of cyclo[18]carbon can be found in reference.[143] For example, the normal mode with a frequency of 361 cm^{-1} is composed in 100% of the deformation coordinate τ_9 (Tau9) and the normal mode of the frequency of 433 cm^{-1} is composed in 86% of the ring breathing coordinate R. There is also a series of doubly degenerated normal modes in the cyclo[18]carbon ring, such as the normal mode of the frequency 539 cm^{-1} (labelled as "a" and "b" in Fig. 4) showing complementary ring puckering motions whereas the normal mode with a frequency of 2293 cm^{-1} presents the complementary ring deformation puckering motions. In contrast, the normal mode with a frequency of 1814 cm^{-1} shows a nondegenerate ring deformation motion. In summary the CNM analysis is a unique tool for decoding important details disguised in the normal modes.[104]

Local force constant guided by bond paths

Another way to derive k^a could be via a topological analysis of the electron density $\rho(\mathbf{r})$[11,144,145] providing a network of BPs, i.e., choosing k^a according to the BPs found between the two monomers. As previously discussed by Kraka and Cremer, a BP can be indicative of a covalent or electrostatic interaction. According to the Cremer–Kraka criterion,[146–148] the necessary condition for a covalent interaction is the existence of a BP and a bond critical point $\mathbf{r}_b$ between two atoms under consideration, and the sufficient condition is a negative local

Can. J. Chem. Downloaded from cdnsciencepub.com by University of Alberta on 09/01/23
For personal use only.

Table 1. Intermonomer distance d, intermonomer local mode force constant k^a, and local mode frequency ω^a without and with projection.

Dimer	Symm.	Mode	d^a (Å)	k^a (mDyn/Å)	$k^{a,p}$ (mDyn/Å)	ω^a (cm^{-1})	$\omega^{a,p}$ (cm^{-1})
MP2/6-311++G(d,p)							
Ar–C_6H_6	C_{6v}	S_x, S_y	0.000	0.097	0.012	80	39
		S_z	3.522	0.036	0.036	49	49
HF–C_6H_6	C_s	S_x	0.377	0.001	0.001	12	9
		S_y	0.217	0.000	0.000	7	5
		S_z	3.119	0.094	0.093	101	100
H_2O–C_6H_6	C_s	S_x	0.127	0.064	0.040	87	77
		S_y	0.000	0.010	0.006	34	30
		S_z	3.253	0.052	0.052	79	78
NH_3–C_6H_6	C_s	S_x	0.153	0.048	0.027	77	79
		S_y	0.265	0.058	0.035	84	87
		S_z	3.443	0.060	0.060	85	85
CH_4–C_6H_6	C_{3v}	S_x, S_y	0.000	0.061	0.030	89	89
		S_z	3.665	0.056	0.056	85	85
LC-B97D3[b]							
Ar–C_6H_6	C_{6v}	S_x, S_y	0.000	0.415	0.066	166	87
		S_z	3.100	0.248	0.248	128	128
B2PLYPD/AVTZ[c]							
C_6H_6–C_6H_6(∥)	C_{2h}	S_x	1.752	0.109	0.070	69	61
		S_y	0.000	0.008	0.004	18	16
		S_z	3.396	0.091	0.081	63	61
C_6H_6–C_6H_6(⊥)	C_s	S_x	0.000	0.052	0.023	48	41
		S_y	0.861	0.288	0.157	112	97
		S_z	4.741	0.097	0.096	65	65

[a]Shift of O_B from the ring midpoint in x direction for S_x and in y direction for S_y, respectively; intermonomer distance $d(O_A, O_B)$ for S_z.
[b]Calculated with the long range-corrected[136] version of the B97 functional plus Grimme's D3BJ dispersion schemes[137] (LC-B97D3) with the def2-TZVPP basis set, and the density fitting approximation.[138]
[c]Grimme's double hybrid functional[139,140] with dispersion correction[141] combined with Ahlrich's AVTZ basis set.

Fig. 3. Structure of planar Ar–C_{18} complex. The S_z mode describing the out of plane motion of the Ar atom in blue color and S_x and S_y modes describing the in plane motion of the Ar atom in x and y directions, respectively, in purple color.

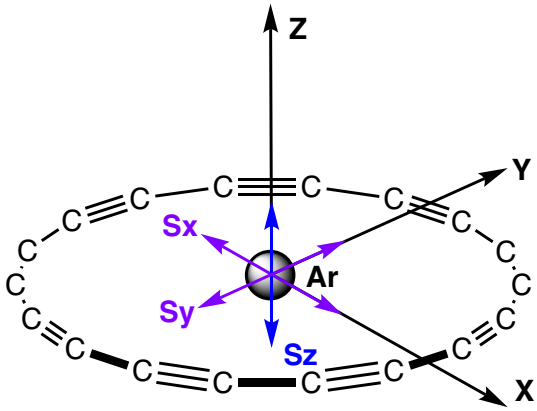

energy density $H(\mathbf{r}_b)$. $H(\mathbf{r})$ is defined as

$$H(\mathbf{r}) = G(\mathbf{r}) + V(\mathbf{r}) \quad (26)$$

where $G(\mathbf{r})$ is the kinetic energy density (always positive) and $V(\mathbf{r})$ is the potential energy density (always negative). $H(\mathbf{r}_b)$ will be close to zero or positive if an interaction is electrostatic or dispersive in nature, often found in the case of weak interactions. It is not uncommon that electrostatic arguments may diverge from observed electron density paths. A thoroughly discussed example,[149–151] is the tetrel bonded complex CF_4–NH_3 which is usually described as being held together by an electrostatic σ–hole interaction between the nitrogen lone pair and the carbon σ–hole collinear to this lone pair, whereas the topological analysis finds three BPs connecting the nitrogen atom to the three fluorine atoms of CF_4. One has also to consider that BPs between distant atoms, e.g., in van der Waals systems, can be preferentially located in electron-rich regions, and as such not necessarily reflecting the overall interactions between the monomers of the van der Waals complex,[152–155] e.g., Clark has shown that electron density paths connecting He or Ne and H_2O are formed even when the interaction is clearly repulsive.

Fig. 4. Decomposition of normal modes into local mode contributions for the Ar–C_{18} complex. Set of local mode parameters used (see legend); S_z, S_x, and S_y describing out of plane and in plane motion of the Ar atom; in plane ring deformation coordinates T and out of plane ring puckering coordinates Q of the cyclo[18]carbon ring; overall ring deformation coordinate τ_9 (Tau9), ring breathing coordinate R. REM in the legend refers to the sum of local mode coordinates with nonsubstantial normal mode contributions. "a" and "b" refer to two degenerate local modes. Further details about the cyclo[18]carbon puckering and deformation coordinates can be found in reference.[143] M06-2X/def2-TZVPP level of theory.

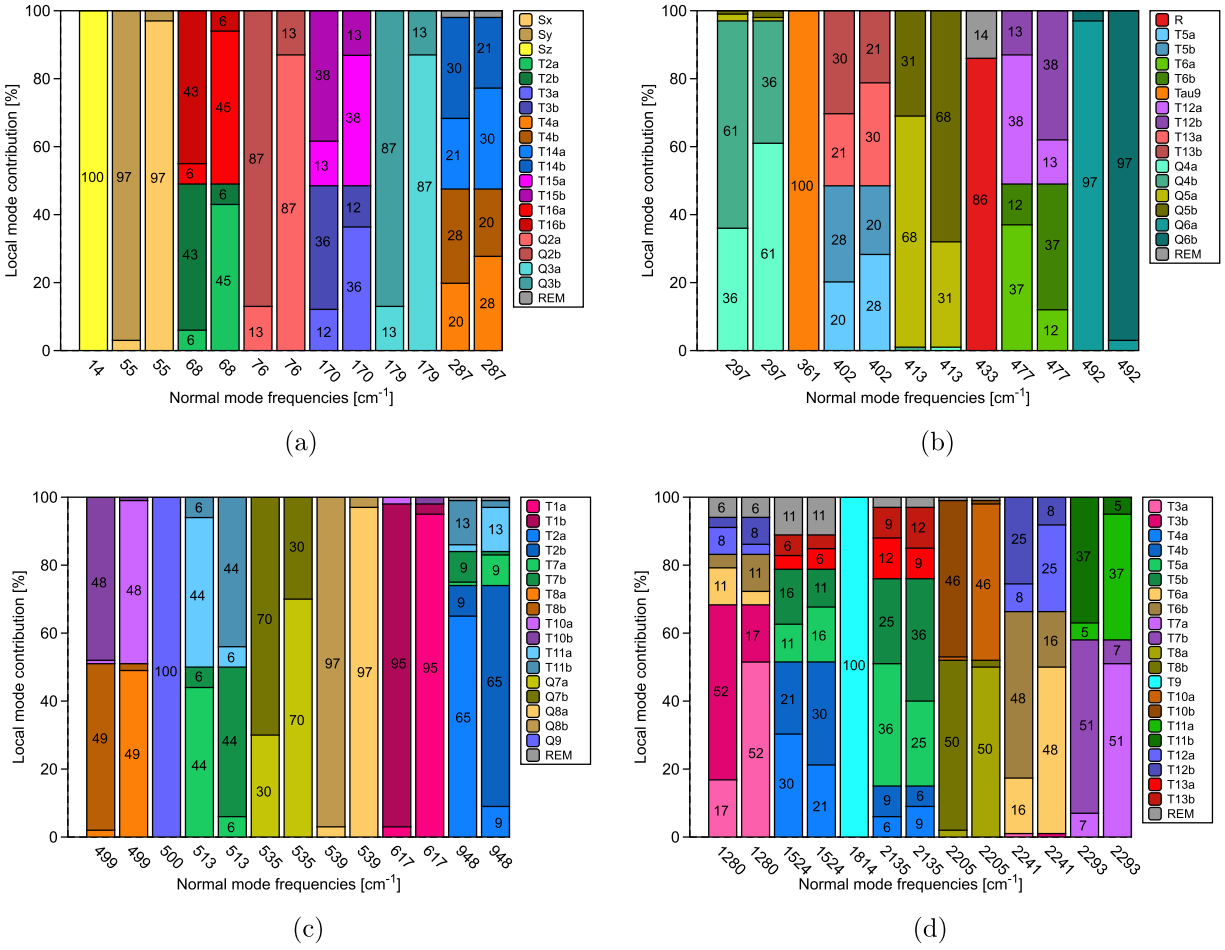

In addition, these electron density paths persist up to 4 Å. The electron density built in the intermonomer region is just a consequence of the distance in these cases.[150] Another prominent example is the phenanthrene/anthracene controversy.[156–158] As shown by Kalescky and co-workers,[156] the 6.8 kcal/mol larger stability of phenanthrene relative to anthracene predominantly results from its higher resonance energy, which is a direct consequence of the topology of ring annelation and not as previously suggested[158] from a BP between the bay H atoms resulting from the proximity of the two H atoms (R(HH) = 2.014 Å). On the other hand, in the case of weak π interactions with longer intermonomer distances, not always a BP is found, as encountered in this study (The BPs found for Group 1–3 complexes are shown in Figs. S2–S7 and BPs for dibenzene (parallel and perpendicular) in Fig. S8 of Supporting Information). To circumvent these problems, some authors have relied on the analysis of the electrostatic potential[159,160] but this approach is also limited, since it does not take into consideration the mutual polarization of the electron density that occurs in the interacting system.[10,149]

Computational details

Group 1 complexes (**1–38**) were calculated with the MP2/6-311++G(d,p) level of theory[161,162] referring to the fact that DFT methods generally underestimate the weak interaction found in these complexes.[163] Group 2 complexes (**39–49**) involve heavy elements such as Ag, Au, and Pt which require a relativistic description, therefore we used the M06/Jorge-DZP/Jorge-TZP-DKH(Me)/NESC model chemistry, where the transition metals were calculated with Jorge-TZP-DKH basis functions of a triple zeta quality,[164] and C, O, and H atoms with a double zeta basis set Jorge-DZP.[165] The M06 functional was used because it is recommended for application in organo- and inorganometallic chemistry and for noncovalent interactions.[166] To include relativistic effects for the heavy elements we used normalized elimination of the small component (NESC), which is an exact two-component relativistic method developed by Dyall.[167,168] NESC was extended in our group[169–176] providing new algorithms for analytical gradients[177,178] and Hessians[179] allowing for all-electron

Can. J. Chem. Downloaded from cdnsciencepub.com by University of Alberta on 09/01/23
For personal use only.

Can. J. Chem. Downloaded from cdnsciencepub.com by University of Alberta on 09/01/23
For personal use only.

relativistic geometry optimization and frequency calculations of large molecules with heavy atoms.[176] For consistency, all transition metal systems in Group 2 were calculated with NESC. In Group 3, we used the M06/6-31G(d,p)[166,180] model chemistry for complexes **58–67** in consistency with the DFT method used in Group 2, combined with a smaller basis set considering the size of the complexes. For the ferrocene complexes in this Group (**50–57**), we used the pure BP86[181] functional with the D3 dispersion correction,[137,182] combined with Dunning's aug-cc-pVTZ basis set,[183–185] instead of the hybrid M06 functional, following suggestions made in a previous study.[186] Group 4 complexes (**68–74**) were calculated with the same PBE0-D3BJ/def2-TZVP[141,187–190] model chemistry as used in reference[103] for consistency. All MP2 and DFT calculations were performed with the GAUSSIAN16 program package,[191] the relativistic NESC calculations with COLOGNE19,[192] and LMA with the LModeA package.[104,193] The topological properties of the electron density were derived from Bader's quantum theory of atoms in molecules approach[194,195] and using the AIMALL program.[196]

Results and discussion

First we summarize overall trends found for the Group 1–4 complexes presented in Fig. 1 then trends within each individual group are presented. Figure 5 defines the intermonomer distances d and local intermonomer force constants $k_n^{a,p}$ for Group 1–3 complexes used in the following discussion. Group 4 intermonomer distances and local force constants are obvious from Fig. 1. For simplicity, k^a is used instead of $k_n^{a,p}$ in the remainder of this work.

Figure 6 presents the correlation between local mode force constant k^a and intermonomer distance d for all complexes shown in Fig. 1 which follows a Badger power relationship[197] to some extent ($R^2 = 0.7131$), i.e., shorter intermonomer distances are related with stronger intermonomer interactions (It has to be noted that not always the shorter bond is the stronger bond[197–199]). The van der Waals complexes of Group I and H-bonding as well as π–hole interactions in Group 4 are on the weaker end of the spectrum with k^a values in the range of 0.1–0.6 (mDyn/Å). Ar–benzene (**1**) is the weakest Group 1 complex with $d = 3.522$ (Å) and $k^a = 0.036$ (mDyn/Å) and Li^+–benzene the strongest Group 1 complex with $d = 1.870$ (Å) and $k^a = 0.555$ (mDyn/Å). Hydrogen bonding in Group 4 complexes **68–73** is considerably stronger than in the water dimer **74**, e.g., $k^a = 0.339$ (mDyn/Å) for **69** compared to $k^a = 0.178$ (mDyn/Å) for **74**, whereas the π–hole interactions, as expected are considerably weaker.[31] Group 2 transition metal hydrides and oxides show stronger interactions with benzene ranging from $k^a = 0.325$ (mDyn/Å) for **49** to $k^a = 1.658$ (mDyn/Å) for **46**. Group 3 compounds show the strongest metal–ring interactions, spanning over a large range with $k^a = 0.960$ (mDyn/Å) for **63** and $k^a = 3.937$ (mDyn/Å) for **52**, the strongest interaction within the hole set. It is interesting to note that Group 3 complexes tend to cluster with the weaker interactions for Ti complexes, followed by Cr and Fe complexes.

In line with these results is the covalent versus electrostatic character of these interactions depicted in Fig. 7, showing the dependency between k^a and $H(\mathbf{r}_b)$. All members of Group 1 are characterized by electrostatic intermonomer interactions as revealed by Fig. 7*a*, π–hole interactions of Group 4 members are borderline, whereas strongest covalent interactions are found for the Fe sandwich complexes. Overall, the $H(\mathbf{r}_b)(k^a)$ relationship is scattered; a few trends can be observed for Groups 2–4 (Fig. 7*b*) but no overall significant correlation, especially not for Group 1 (see Fig. 7*a*). These departures can be attributed to the problem that in a dimer system with π interactions, multiple bond critical points between the two monomers may be found, whose properties, cannot be well compared with a measure taken directly between the two interacting monomers. In summary, the local intermonomer force constant provides a chemically meaningful measure of interaction strength, describing intermonomer interactions in a seamless way, over a large range from weak electrostatic to strong covalent bonding.

Group 1

Complexes **1–38** involve the interaction of an atom/small molecule with the π electrons of benzene or substituted benzenes. The π interaction in Ar–benzene **1** has a k^a value 0.036 mDyn/Å which becomes slightly smaller for the mono- and ortho-difluoro-substituted complexes **2** and **3** (0.032 and 0.036 mDyn/Å, respectively), whereas for meta- and para-difluoro-substituted complexes **4** and **5** the local mode force constant increases (0.040 and 0.043 mDyn/Å, respectively). Substitution of benzene with fluorine is expected to decrease the benzene π electronic density leading to increased van der Waals attraction of Ar, because of a decrease in electron repulsion between the electron-rich Ar atom and the π system of benzene. This is the case for the para difluoro-substituted complex **5** (0.043 mDyn/Å), where the Ar atom is positioned over the benzene ring center. In complexes **2** and **3** the Ar is shifted away from the benzene center, and as a result there is a stronger electron repulsion between the electrons of the Ar atom and the π electrons of the ring, leading to a smaller interaction. This also holds for **4** but to a lesser extent than for **3**. In **4** there is a competition between the electron withdrawing effect of two fluorine atoms making the π interaction stronger, and the electron repulsion effect making the π interaction weaker, which as a final effect results in a force constant close to that of the unsubstituted benzene complex **1**. Cationic complexes as **7** and **9** show as expected a stronger interaction.

The interaction between acetylene and the π system of benzene with the acetylene arranged perpendicular to the benzene ring and interacting via a hydrogen atom involve complexes **18–26**, with **19–22** focusing on fluorine substitution and **23–26** on methyl substitution of the benzene complexes. The unsubstituted acetylene complex **18** has a k^a value of 0.105 mDyn/Å which becomes smaller for complexes with the mono- and difluoro-substituted complexes (0.100–0.057 mDyn/Å). The para difluoro-substituted complex **20** and the trifluoro-substituted complex **22** are found on the stronger end (0.093 and 0.082 mDyn/Å, respectively) because the acetylene is located over the ring center increasing the electrostatic attraction between the benzene π cloud and the

Fig. 5. Intermonomer distance d and local intermonomer force constants $k_n^{a,p}$ used in the work.

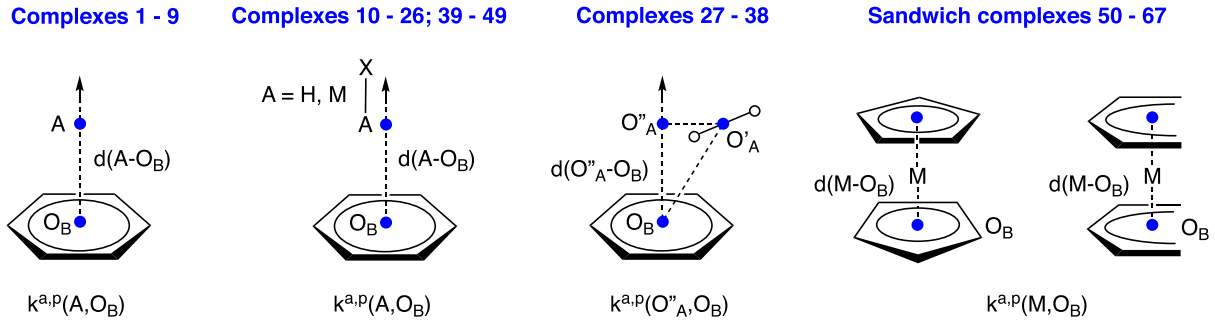

Fig. 6. Correlation between local mode force constant k^a and intermonomer distance d, as defined in Fig. 5. Group 1: van der Waals complexes (orange color); Group 2: transition metal complexes (blue color); Group 3: ferrocenes (green color), Cr sandwich complexes (red color), Ti sandwich complexes (purple color); Group 4 complexes olive color. The two different data sets of M–O_B interactions for Group 3 complexes **52–57** as well as π–hole and H-bonding interactions for Group 4 complexes **69–71** are labelled as (a) and (b), see Fig. 1. For model chemistries used, see "Computational details".

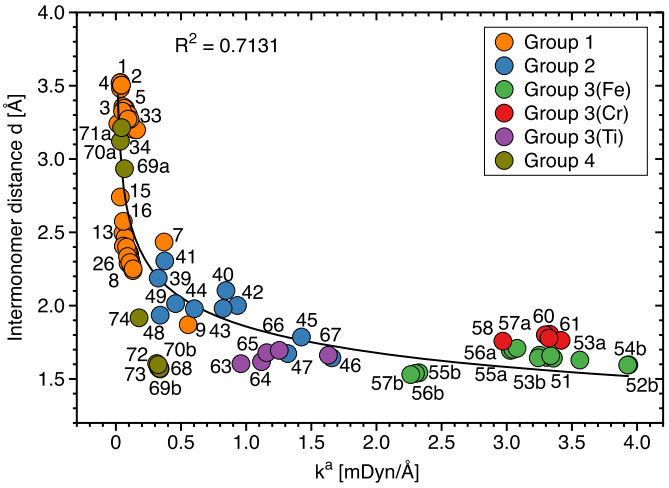

positively charged hydrogen of acetylene. This indicates that the orientation of entire acetylene relative to the benzene center influences the strength of the π interaction. The largest k^a (0.132 mDyn/Å) is observed in this series for the trimethyl-substituted complex **26** compared to the unsubstituted complex **18**. The two dimethyl-substituted complexes **24** and **25** have smaller force constants (0.122 and 0.108 mDyn/Å, respectively). In **25** the acetylene molecule is tilted relative to the benzene ring making the π interaction weaker, while in **24** the acetylene molecule is perpendicular to the benzene ring with the stronger π interaction. In the monomethyl-substituted complex **23** the acetylene tilting is large enough to reduce the electron-donating effect of the methyl group, and as a consequence k^a (0.089 mDyn/Å) becomes smaller than that of the unsubstituted complex **18**.

In complexes **27–38** ethylene and acetylene are oriented parallel to the benzene ring. Complexes **32–34** show the effect of fluorine substitution of the ethylene molecule with k^a values of 0.115, 0.135, 0.159 mDyn/Å, respectively for the di-, tri-, and quadro-fluorination, which exceed the k^a of the unsubstituted ethylene complex **27** (0.073 mDyn/Å) considerably. Fluorine substitution decreases the electron density of the ethylene π bond decreasing in turn the electron repulsion between the π systems of ethylene and benzene leading to a stronger interaction. This effect parallels fluorine substitution of methane in the methane–benzene complex **16** and the trifluoro-substituted methane–benzene complex **17** (k^a = 0.057 versus 0.117 mDyn/Å). Fluorination make the methane hydrogen more positive, increasing its electrostatic attraction with the benzene ring. Along these lines, cationic complexes **7** and **9** (k^a values of 0.370 and 0.555 mDyn/Å, respectively) show therefore as expected—the strongest interaction found for Group **1** complexes. In summary, the interaction strength in these complexes is influenced by benzene ring substitution, the nature and orientation of the ligand interacting with the benzene ring, together determining the competition between van der Waals attraction and the electrostatic repulsion between benzene π and ligand electrons. This is all well captured by the S_z parameter.

It has to be noted that whereas the force constants for a perpendicular versus parallel arrangement of acetylene and benzene (complexes **18–26** and **35–36**) are similar, the corresponding local mode frequencies are not, as revealed by the data in Fig. 1. This is a result of different definition of the masses specifying the interaction between monomer A and ring B. In **18** with the interaction via one of the acetylene hydrogen atoms the hydrogen mass (m = 0.994 amu) is taken for monomer A whereas in **35** or **36** the center of mass of acetylene is taken (m = 19.11 amu). This mass enters eqs. 18 and 19 determining the local mode frequency. This clearly shows that local mode force constants which are independent on the mass are the better suited bond strength descriptor.

Group 2

Complexes **39–49** involve the interaction of the benzene π system with a transition metal hydride and/or oxide. According to our calculations for most Group 2 complexes a π

Can. J. Chem. Downloaded from cdnsciencepub.com by University of Alberta on 09/01/23
For personal use only.

Fig. 7. Dependency between local mode force constant k^a and $H(\mathbf{r}_b)$. (*a*) Group 1: van der Waals complexes (orange color); (*b*) Group 2: transition metal complexes (blue color); Group 3: ferrocenes (green color), Cr sandwich complexes (red color), Ti sandwich complexes (purple color); Group 4 complexes olive color. The two different data sets of M–O_B interactions for Group 3 complexes **52–57** as well as π–hole and H-bonding interactions for Group 4 complexes **69–71** are labelled as (a) and (b), see Fig. 1. For model chemistries used, see "Computational details".

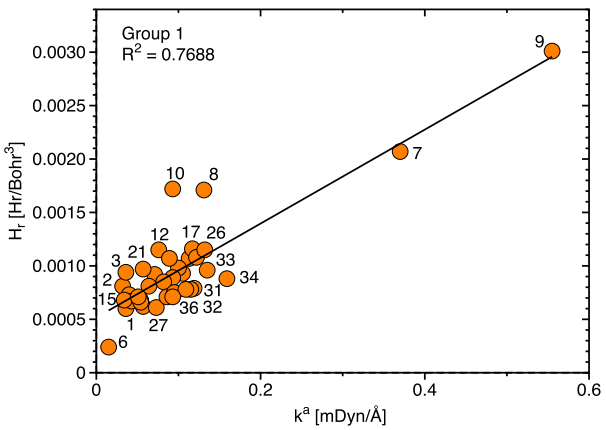

(a)

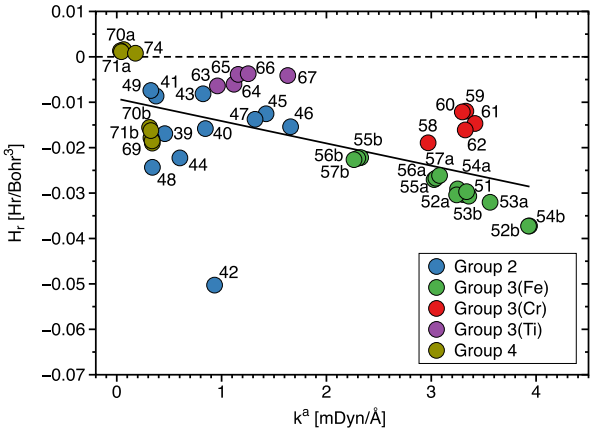

(b)

complex between the metal and one of the C–C ring bonds is formed, which moves the metal atom away from the benzene center (see BPs in Figs. S5 and S6 of Supporting Information). Exceptions are the CoO–benzene **46** and the NiO–benzene complex **47** exhibiting C_{6v} symmetry, i.e., the metal oxide is located above the benzene ring center. As indicated by the negative $H(\mathbf{r}_b)$ values, the interaction is covalent for all members of that group. Local mode force constants in this series are in a range between 0.3 and 1.7 mDyn/Å, which indicates that the strength of the π interaction of these complexes is smaller than that found for ferrocenes force constant values in the range between 2.3 and 4.0 mDyn/Å. On the other hand, the transition metal hydrides and oxides form stronger π interactions with benzene than the Cr and Ti sandwich complexes, which is indicated by more negative $H(\mathbf{r}_b)$ values, as shown in Fig. 7*b*. Overall, the specific strength of the π interaction in Group 2 complexes depends on the character of the metal atom, i.e., its electron configuration, polarizability, and the different net charge of the metal atom.

We also tested for this group the bond disassociation energy (BDE)[200–202] as an alternative measure of the interaction strength and how it relates to our local mode force constant. However, it has to be noted that the BDE is a reaction parameter that includes all changes taking place during the dissociation process. Accordingly, it includes any (de)stabilization effects of the fragments to be formed. It reflects the energy needed for bond breaking, but also contains energy contributions due to geometry relaxation and electron density reorganization in the dissociation fragments. Therefore, the BDE is not a suitable measure of the intrinsic strength of a chemical bond and its use may lead to misjudgments, as documented in the literature.[74,149,203–206] This is reflected by the weak correlation of local mode force constant k^a and the BDE for Group 2 complexes shown in Fig. 8. Although in these complexes reorganization of the electron density and geometry

Fig. 8. Correlation between local mode force constant k^a and bond dissociation energy (BDE) for complexes of Group 2. For model chemistries used, see "Computational details".

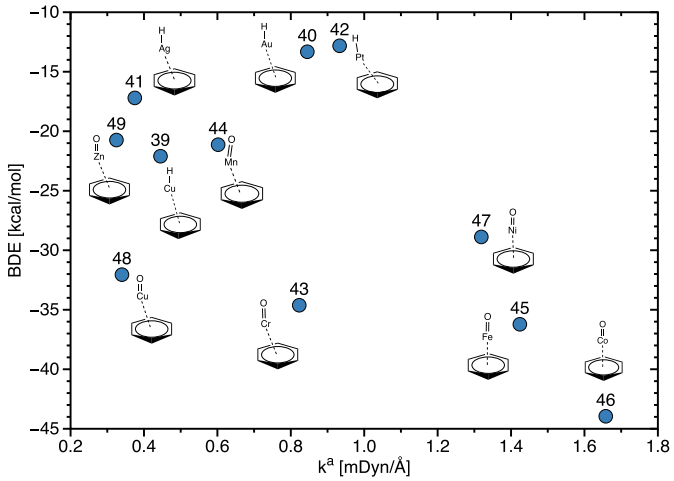

relaxation is expected to be small, there is no significant overall correlation between these two properties. What we find is a clustering of similar complexes, such as for the NiO–, FeO–, and CoO–benzene complexes **47**, **45**, and **46**; or the AgH–, AuH–, and PtH–benzene complexes **41**, **40**, and **42**.

Group 3

Complexes**50–67** involve ferrocenes **50–57**, chromocenes **58**, **61**, **62**, two Cr–benzene reference complexes **59**, **60**, and Ti sandwich compounds **63–67**. Metal–ligand bonding in metallocenes involves the metal 3*d* electrons interacting with the π electrons of the two Cp rings.[207] In the field of the Cp

Can. J. Chem. Downloaded from cdnsciencepub.com by University of Alberta on 09/01/23
For personal use only.

Can. J. Chem. Downloaded from cdnsciencepub.com by University of Alberta on 09/01/23
For personal use only.

ligands the 3d orbitals of the metal split up into two degenerate e_2', followed by an a_1', and two higher lying e_2'' orbitals which combine with Cp^{2-} framework orbitals. According to MO theory, metal–ligand bonding is predominately due to the stabilization of the e_1'' π orbitals of the Cp ligands through combination with the e_2' metal d orbitals ($3d_{xz}$ and $3d_{yz}$ when the z axis coincides with the fivefold symmetry axis).[208] This leads in ferrocenes with four of the six Fe 3*d* electrons occupying the e_2' orbitals to the strongest ligand–metal interactions, followed by chromocenes with only three of the four Cr 3*d* electrons occupying e_2' orbitals (one electron occupies the a_1' following Hund's rule of maximum multiplicity) with the weakest metal–ligand interaction for Ti sandwich complexes, because Ti has only two 3*d* electrons.[207] These MO-based considerations are fully in line with our results presented in Figs. 6 and 7*b*.

In addition to changing the metal atom, the strength of the metal–ligand π interaction in metallocenes can be modified via Cp ring substituents or replacement of the Cp carbons with heteroatoms. For example, the Fe–Cp interaction in ferrocene can be strengthened by replacing all Cp hydrogen atoms with fluorine, thus increasing the ring π density, as realized in ferrocene complex **52**, increasing k^a from 3.305 mDyn/Å in ferrocene **50** to 3.937 mDyn/Å, the strongest sandwich complex of Group 3. This is in line with experimental and theoretical data of substituted ferrocenes[209,210] suggesting that electron accepting substituent leads to a larger overlap between the iron *d* orbitals and the Cp orbitals, while the electron-donating substituent results in less iron *d* to Cp mixing. It is also interesting to notice that the k^a value of the unsubstituted Cp of complex **52** becomes smaller (3.251 mDyn/Å). This indicates that while fluorine substitution increases orbital mixing between the fluorinated Cp and Fe *d* orbitals at the same time the orbital mixing between the unsubstituted Cp and the Fe *d* orbitals decreases, as a result of electronic density transfer within the Fe *d* orbitals in a direction of the substituted Cp. Substitution of Cp with methyl groups as realized in **53**, has a similar although smaller effect as reflected by a k^a value of 3.561 mDyn/Å, and a k^a value of 3.242 mDyn/Å for the interaction with the unsubstituted Cp ring. Combining both, i.e., fluorination of one CP ring and methyl substitution of the other as realized in **54** leads to a slight decrease of both the fluoro-substituted and the methyl-substituted Cp ring force constants (3.928 and 3.337 mDyn/Å). One way to weaken the intermonomer interaction is to replace all C ring atoms with P decreasing the ring π density, as realized in ferrocene complex **56** leading to a k^a value of 2.299 mDyn/Å, the smallest value found for Group 3 complexes. Complexes **55–57** show the effect of combining a methyl-substituted Cp with the pentaphospha–Cp ring. By increasing the number of the methyl group substitution in the Cp ring k^a increases from 3.027 mDyn/Å for the unsubstituted Cp in **55**, through 3.047 mDyn/Å for the dimethyl-substituted Cp ring in **56** to 3.079 mDyn/Å for the pentamethyl-substituted Cp ring in **57**. Similarly, the value k^a decreases for the pentaphospha–Cp ring from 2.326 mDyn/Å for the reference complex **55** through 2.299 mDyn/Å for the dimethyl-substituted Cp ring in **56** to 2.263 mDyn/Å for the pentamethyl-substituted CP ring in **57**. These results clearly show the complex interplay of ring substitution on the intermonomer interaction strength in ferrocenes, perfectly monitored by the local force constant.

Fig. 9. The iso-surface of electron density for weak (**57**), medium (**51**), and strong (**52**) ferrocenes. The surface was generated using the independent gradient model[211] with the iso-surface value of 0.02.

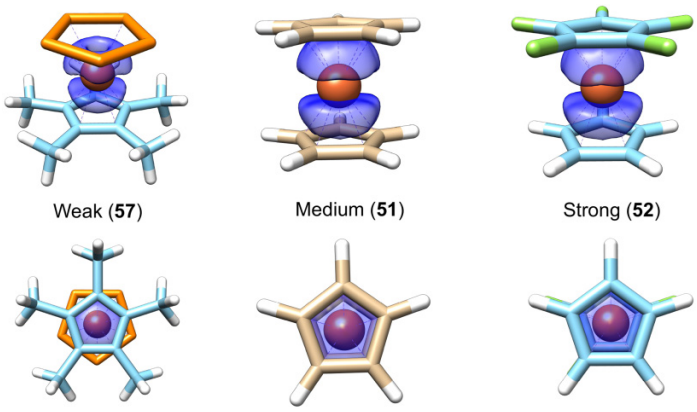

The resulting change in the intermonomer electron density can be visualized via the iso-surface of electron density as shown in Fig. 9 comparing the three surfaces for weak (**57**), medium (**51**), and strong (**52**) ferrocene. According to Fig. 9 we observe an increase in the total electron density between the metal and the π system of the Cp rings for the strong ferrocene (**52**) when compared with the electron density in this region of the weak (**57**) ferrocene, which is consistent with the values of the local mode force constants of these complexes (2.263/3.079 and 3.937/3.251 mDyn/Å for the **57** and **52** complexes, respectively).

As discussed above chromocene **58** has a weaker metal–ligand interaction than ferrocene with a k^a of 2.970 mDyn/Å compared to the ferrocene value of 3.358 mDyn/Å. Complexes **59** and **60** show the effect of a phosphorus ligand $P(OMe)_3$ on the π interaction between Cr and a single Cp ring. Substitution of the CO ligand in **59** with $P(OMe)_3$ as realized in **60** slightly decreases k^a from 3.330 to 3.296 mDyn/Å indicating that σ electron-donating ligands decrease the π interaction between Cr and the Cp ring. It is interesting to note that bending increases the metal–Cp interaction as reflected by the increased k^a values of complexes **61** and **62** (3.417 and 3.324 mDyn/Å, respectively) compared to the chromocene reference value of 2.970 mDyn/Å. Bending the Cp rings increases the overlap between the Cp ring π orbitals from the ring and the Cr *d* orbitals, which results with a stronger π interaction. Replacing one hydrogen atom in **61** with a silyl group, **62**, lowers the π interaction between Cr and the Cp rings, which is most likely a steric effect of the bulky SH_3 group being located between the rings.

Sandwich complexes involving Ti and two U-shaped 2,4-dimethylpentadienyl ligands are shown in **63–67**. In particular the effects of σ electron donation to the metal from the thee phosphorus ligands $P(Me)_3$, $P(OEt)_3$, and PF_3, are presented in complexes **65**, **66**, and **67**, respectively. We observe an increase in k^a from 1.158, through 1.254, to

Can. J. Chem. Downloaded from cdnsciencepub.com by University of Alberta on 09/01/23
For personal use only.

1.631 mDyn/Å for **65**, **66**, and **67** respectively, which is in line with the decreasing σ electron donation character of these three phosphorus ligands. As the atom attached to the P atom in the phosphorus ligands becomes more electronegative, the empty P–X σ^* orbital becomes more stable making it a better acceptor of electron density from the metal. Therefore, the PF_3 phosphorus ligand shows also a σ^* back donation effect accepting electrons from the metal. According to our results, the strength of the π interaction between Ti and dimethylpentadienyl ligands becomes stronger with a weaker σ electron-donating ligand, and in the case of PF_3 which additionally accepts electrons from the metal, the strength of the complex **67** (1.631 mDyn/Å) becomes even larger than in the phosphorus-free ligand complex **64** (1.118 mDyn/Å).

Group 4

To diversify our test set we included in Group 4 a simplified model of the gallic acid dimer complex **68** probing the recently suggested oxygen–π hole interactions in addition to in-plane hydrogen bonding when exposed to ether **69**, ketone **70** or fluorosubstituted ether **71**,[103] as well as formic and acetic acid dimer **72** and **73** and the water dimer **74** as references for the in-plane hydrogen bonds. There has been an increasing interest over the last years in noncovalent interactions based on the presence of electron-depleted regions, so-called σ or π holes, with high directionality and strength, comparable to hydrogen bonds.[212,213] Although the popular molecular electrostatic potential approaches[214,215] provide qualitative insight, there is a need for a more rigorous quantification considering the fact that besides a strong electrostatic component other factors contribute to the strength of these interactions, such as polarization and charge transfer effects, complemented by dispersive forces, just to name a few. In this work we used the local intermonomer force constant k^a for this purpose, which already has turned out as an efficient tool to assess the π–hole interaction strength between aryl donors and small molecule acceptors.[31]

As shown by the data in Fig. 1 the oxygen–π hole interactions in **69–71** are considerably weaker than the in-plane hydrogen bonds ranging from $k^a = 0.066$, through 0.035 to 0.044 mDyn/Å, respectively compared to the corresponding hydrogen bonds ranging from $k^a = 0.339$, through 0.326–0.337 mDyn/Å, respectively. This is also reflected in the interaction distances, being on the order of 2.9–3.2 Å for the oxygen–π hole interactions compared to 1.6–1.9 Å for the hydrogen bonds. Replacing the methyl hydrogen atoms of the ether with fluorine atoms as realized in **71** slightly weakens the oxygen–π hole interaction as well as replacing dimethlyether with acetone. The effect on the in plane hydrogen bond is marginal. Compared to hydrogen bonding in the water dimer **74** in all dimer complexes **68–73** the hydrogen bond strength is strongly increased by double hydrogen bonding,[124] as reflected by the shorter distances and larger force constants (d in the range of 1.5–1.6 Å compared to 1.9 Å for the water dimer; k^a in the range of 0.32–0.34 mDyn/Å compared with 0.18 mDyn/Å). Overall, these results show that the local intermonomer force constant has a broad spectrum including also π hole interactions and their comparison with conventional hydrogen bonding.

Conclusions

In this study we developed and tested the new local mode parameter for a precise description of the intermolecular π interaction between two monomers. It was derived from the set of nine possible intermonomer normal modes. One of the three intermonomer normal stretching modes included in this set, the S_z mode, corresponds to the genuine stretching between the monomers, thus reflecting the intermolecular interaction between these two monomers. Our study identified the local mode force constant k^a connected with the S_z mode as a qualified measure of the strength of this intermonomer interaction, outperforming other approaches describing these interactions with averaged force constants or force constants guided by the BPs of the electron density. The new parameter was tested for a diverse set of molecular complexes, which was divided into four groups. Group 1 included atoms, ions, and small molecules interacting with benzene and substituted benzenes. Group 2 included transition metal hydrides and oxides interacting with benzene, while Group 3 involved ferrocenes, chromocenes, and titanium sandwich compounds. Group 4 presents an extension to oxygen–π hole interactions in comparison with in-plane hydrogen bonding.

We found that the strength of the π interactions in these diverse molecular clusters can vary from weak interactions with predominantly of electrostatic character, such as between argon and benzene, to strong interactions with a substantial covalent nature, all being seamlessly described and compared with the new intermonomer local mode force constant, developed in this work.

Acknowledgements

This work was financially supported by the National Science Foundation (Grant No. CHE 2102461). We thank SMU's Center for Scientific Computing for providing generous computational resources. WZ acknowledges the support by the National Natural Science Foundation of China (NSFC, Grant No. 22073072).

Article information

History dates

Received: 28 September 2022
Accepted: 9 November 2022
Accepted manuscript online: 16 December 2022
Version of record online: 23 May 2023

Notes

This paper is one of a selection of papers from the 12th Triennial Congress of the World Association of Theoretical and Computational Chemists (WATOC 2020).

Copyright

© 2022 The Author(s). Permission for reuse (free in most cases) can be obtained from copyright.com.

Can. J. Chem. Downloaded from cdnsciencepub.com by University of Alberta on 09/01/23
For personal use only.

Data availability

Data generated or analyzed during this study are provided in full within the published article and its supplementary materials.

Author information

Author ORCIDs

Elfi Kraka https://orcid.org/0000-0002-9658-5626

Author contributions

Conceptualization, EK
Data curation, WZ, MF, VO, YT
Formal analysis, MF, VO, YT, EK
Funding acquisition, EK
Investigation, WZ, MF, VO, YT, EK
Methodology, WZ, EK
Project administration, EK
Resources, EK
Software, WZ
Supervision, EK
Validation, VO, EK
Visualization, MF
Writing – original draft, WZ, MF, EK
Writing – review & editing, EK

Competing interests

The authors declare there are no competing interests.

Supplementary material

Supplementary data are available with the article at https://doi.org/10.1139/cjc-2022-0254.

References

(1) Juanes, M.; Saragi, R. T.; Caminati, W.; Lesarri, A., Chem. Eur. J. **2019**, *25*, 1–11. doi:10.1002/chem.201901113.
(2) Maji, R.; Wheeler, S. E. In *Applied Theoretical Organic Chemistry*; D., Tantillo, Ed.; World Scientific: New York, **2018**; pp. 289–320. doi:10.1142/9781786344090_0010.
(3) Neel, A. J.; Hilton, M. J.; Sigman, M. S.; Toste, F. D., Nature **2017**, *543*, 637–646. doi:10.1038/nature21701.
(4) Stöhr, M.; Voorhis, T. V.; Tkatchenko, A., Chem. Soc. Rev. **2019**, *48*, 4118–4154. doi:10.1039/C9CS00060G.
(5) Hermann, J.; Tkatchenko, A., Chem. Rev. **2017**, *117*, 4714–4758. doi:10.1021/acs.chemrev.6b00446.
(6) Bereau, T.; DiStasio, R. A.; Tkatchenko, A.; von Lilienfeld, O. A., J. Chem. Phys. **2018**, *148*, 241706. doi:10.1063/1.5009502.
(7) Mahadevi, A. S.; Sastry, G. N., Chem. Rev. **2016**, *116*, 2775–2825. doi:10.1021/cr500344e.
(8) *Noncovalent Forces*; S., Scheiner, Ed.; Springer: New York, **2015**. doi:10.1007/978-3-319-14163-3.
(9) Chen, J.; Peng, Q.; Peng, X.; Zhang, H.; Zeng, H., Chem. Rev. **2022**, *122*, 14594–14678. doi:10.1021/acs.chemrev.2c00215.
(10) Oliveira, V.; Cremer, D.; Kraka, E., J. Phys. Chem. A **2017**, *121*, 6845–6862. doi:10.1021/acs.jpca.7b06479.
(11) Oliveira, V. P.; Marcial, B. L.; Machado, F. B. C.; Kraka, E., Materials **2020**, *13*, 55. doi:10.3390/ma13010055.
(12) Tao, Y.; Qiu, Y.; Zou, W.; Nanayakkara, S.; Yannacone, S.; Kraka, E., Molecules **2020**, *25*, 1589. doi:10.3390/molecules25071589.
(13) Yannacone, S.; Sethio, D.; Kraka, E., Theor. Chem. Acc. **2020**, *139*, 125. doi:10.1007/s00214-020-02631-x.
(14) *Noncovalent Interactions in Catalysis,Catalysis Series*; K. T., Mahmudov, M. N., Kopylovich, M. F. C., Guedes da Silva, A. J. L., Pombeiro, Ed.; The Royal Society of Chemistry, **2019**; p P001–653. doi:10.1039/9781788016490-FP001.
(15) Kim, K. S.; Tarakeshwar, P.; Lee, J. Y. M., Chem. Rev. **2000**, *100*, 4145–4185. doi:10.1021/cr990051i.
(16) Zhang, Y.; Chen, S.; Ying, F.; Su, P.; Wu, W., J. Phys. Chem. A **2018**, *122*, 5886–5894. doi:10.1021/acs.jpca.8b04201.
(17) Kuzniak-Glanowska, E.; Glanowski, M.; Kurczab, R.; Bojarski, A. J.; Podgajny, R., Chem. Sci. **2022**, *13*, 3984–3998. doi:10.1039/D2SC00763K.
(18) Di, Y.-M.; Li, M.-H.; Zhang, S.-Q.; You, M.-H.; Lin, M.-J., Cryst. Growth Des. **2021**, *21*, 3511–3520. doi:10.1021/acs.cgd.1c00288.
(19) Luo, N.; Ao, Y.-F.; Wang, D.-X.; Wang, Q.-Q., Angew. Chem. Int. Ed. **2021**, *60*, 20650–20655. doi:10.1002/anie.202106509.
(20) Maynard, J. R. J.; Galmés, B.; Stergiou, A. D.; Symes, M. D.; Frontera, A.; Goldup, S. M., Angew. Chem. Int. Ed. **2022**, *61*, e202115961. doi:10.1002/anie.202115961.
(21) Breugst, M.; von der Heiden, D.; Schmauck, J., Synthesis **2017**, *49*, 3224–3236. doi:10.1055/s-0036-1588838.
(22) Frontera, A.; Gamez, P.; Mascal, M.; Mooibroek, J. T.; Reedijk, J., Angew. Chem. Int. Ed. **2011**, *50*, 9564–9583. doi:10.1002/anie.201100208.
(23) Quinonero, D.; Frontera, A., Science **2022**, *4*.
(24) Makuvaza, J. T.; Kokkin, D. L.; Loman, J. L.; Reid, S. A., J. Phys. Chem. A **2019**, *123*, 2874–2880. doi:10.1021/acs.jpca.9b01020.
(25) Shin, M.; Park, Y.; Jin, S.; Jung, Y. M.; Cha, H. J., Chem. Mater. **2021**, *33*, 3196–3206. doi:10.1021/acs.chemmater.1c00079.
(26) Aydin, F.; Moradzadeh, A.; Bilodeau, C. L.; Lau, E. Y.; Schwegler, E.; Aluru, N. R.; Pham, T. A., J. Chem. Theory Comput. **2021**, *17*, 1596–1605. doi:10.1021/acs.jctc.0c00827.
(27) Tan, G.; Wang, Y.; He, Y.; Miao, G.; Li, Y.; Wang, X., J. Control. Release **2022**, *349*, 486–501. doi:10.1016/j.jconrel.2022.07.016.
(28) Zhang, X.; Dai, H.; Yan, H.; Zou, W.; Cremer, D., J. Am. Chem. Soc. **2016**, *138*, 4334–4337. doi:10.1021/jacs.6b01249.
(29) Zou, W.; Zhang, X.; Dai, H.; Yan, H.; Cremer, D.; Kraka, E., J. Organometal. Chem. **2018**, *856*, 114–127. doi:10.1016/j.jorganchem.2018.02.014.
(30) Savastano, M.; García-Gallarín, C.; López de la Torre, M. D.; Bazzicalupi, C.; Bianchi, A.; Melguizo, M., Coord. Chem. Rev. **2019**, *397*, 112–137. doi:10.1016/j.ccr.2019.06.016.
(31) Yannacone, S.; Freindorf, M.; Tao, Y.; Zou, W.; Kraka, E., Crystals **2020**, *10*, 556. doi:10.3390/cryst10070556.
(32) Wheeler, S. E.; Seguin, T. J.; Guan, Y.; Doney, A. C., Acc. Chem. Res. **2016**, *49*, 106–1069. doi:10.1021/acs.accounts.6b00096.
(33) Seguin, T. J.; Wheeler, S. E., CS Catal. **2016**, *A6*, 7222–7228.
(34) Shah, R. A.; Ostertag, T. W.; Tang, S.; Dziubla, T. D.; Hilt, J. Z., J. Appl. Polym. Sci. **2021**, *138*, 50257. doi:10.1002/app.50257.
(35) Thakuria, R.; Nath, N. K.; Saha, B. K., Cryst. Growth Des. **2019**, *19*, 523–528. doi:10.1021/acs.cgd.8b01630.
(36) Makoś, M. Z.; Zou, W.; Freindorf, M.; Kraka, E., Mol. Phys. **2020**, *118*, e1768314. doi:10.1080/00268976.2020.1768314.
(37) Fan, Q.; Fu, J.; Li, H.; Feng, H.; Sun, W.; Xie, Y.; King, R. B.; Schaefer, H. F., Phys. Chem. Chem. Phys. **2018**, *20*, 5683–5691. doi:10.1039/C7CP07379H.
(38) Bau, M. A.; Wiesler, S.; Younas, S. L.; Streuff, J., Chem. Eur. J. **2019**, *25*, 1–16. doi:10.1002/chem.201901505.
(39) Arias-Olivares, D.; Paez-Hernandez, D.; Islas, R., New J. Chem. **2018**, *42*, 5334–5344. doi:10.1039/C8NJ00510A.
(40) Kealy, T. J.; Pauson, P. L., Nature **1951**, *168*, 1039–1040. doi:10.1038/1681039b0.
(41) Miller, S. A.; Tebboth, J. A.; Tremaine, J. F., J. Chem. Soc. **1952**, *114* 632–635. doi:10.1039/jr9520000632.
(42) Durand, D. J.; Fey, N., Chem. Rev. **2019**, *119*, 6561–6594. doi:10.1021/acs.chemrev.8b00588.
(43) Ahn, S.; Hong, M.; Sundararajan, M.; Ess, D. H.; Baik, M.-H., Chem. Rev. **2019**, *119*, 6509–6560. doi:10.1021/acs.chemrev.9b00073.
(44) Parker, P. M., *The 2021–2026 World Outlook for Metallocene Polyethylenes*; ICON Group International, Inc.: New York, **2020**.
(45) Liu, C.-X.; Gu, Q.; You, S.-L., Trend. Chem. **2020**, *2*, 737–749. doi:10.1016/j.trechm.2020.05.003.
(46) Cao, L.; Yan, X.; Xi, C., Coord. Chem. Rev. **2020**, *416*, 213330. doi:10.1016/j.ccr.2020.213330.

Can. J. Chem. Downloaded from cdnsciencepub.com by University of Alberta on 09/01/23
For personal use only.

(47) Kaminsky, W., Rend. Lincei Sci. Fis. Nat. **2017**, *28*, 87–95. doi:10.1007/s12210-016-0588-5.
(48) Gu, H.; Ciganda, R.; Gatard, S.; Lu, F.; Zhao, P.; Ruiz, J.; Astruc, D., J. Organomet. Chem. **2016**, *821*, 54–61. doi:10.1016/j.jorganchem.2016.09.012.
(49) Gerasimova, T. P.; Katsyuba, S. A., J. Organomet. Chem. **2015**, *776*, 30–34. doi:10.1016/j.jorganchem.2014.10.042.
(50) Hailes, R. L. N.; Oliver, A. M.; Gwyther, J.; Whittell, G. R.; Manners, I., Chem. Soc. Rev. **2016**, *45*, 5358–5407. doi:10.1039/C6CS00155F.
(51) Arias-Olivares, D.; Páez-Hernández, D.; Islas, R., New J. Chem. **2018**, *42*, 5334–5344. doi:10.1039/C8NJ00510A.
(52) Buades, A. B.; Arderiu, V. S.; Maxwell, L.; Amoza, M.; Choquesillo-Lazarte, D.; Aliaga-Alcalde, N.; Viñas, C.; Teixidor, F.; Ruiz, E., ChemComm **2019**, *55*, 3825–3828.
(53) Santos, M. M.; Bastos, P.; Catela, I.; Zalewska, K.; Branco, L. C., Mini Rev. Med. Chem. **2017**, *17*, 771–784. doi:10.2174/1389557516666161031141620.
(54) Ismail, M. K.; Horswell, S. L.; Hodges, N. J.; Armstrong, K. A.; Hodder, S. L.; Male, L.; Nguyen, H. V.; Wilkinson, E. A.; Tucker, J. H. R., Dalton Trans. **2020**, *49*, 1181–1190. doi:10.1039/C9DT04174E.
(55) Wirtz, L.; Schäfer, A., Chem. Eur. J. **2021**, *27*, 1219–1230. doi:10.1002/chem.202003161.
(56) Bau, M. A.; Wiesler, S.; Younas, S. L.; Streuff, J., Chem. Eur. J. **2019**, *25*, 10531–10545. doi:10.1002/chem.201901505.
(57) Berryman, V. E. J.; Shephard, J. J.; Ochiai, T.; Price, A. N.; Arnold, P. L.; Parsons, S.; Kaltsoyannis, N., Phys. Chem. Chem. Phys. **2020**, *22*, 16804–16812. doi:10.1039/D0CP02947E.
(58) Arnold, P. L.; Ochiai, T.; Lam, F. Y. T.; Kelly, R. P.; Seymour, M. L.; Maron, L., Nat. Chem. **2020**, *12*, 654–659. doi:10.1038/s41557-020-0457-9.
(59) Xemard, M.; Zimmer, S.; Cordier, M.; Goudy, V.; Ricard, L.; Clavaguera, C.; Nocton, G., J. Am. Chem. Soc. **2018**, *140*, 14433–14439. doi:10.1021/jacs.8b09081.
(60) Walter, O., Chem. Eur. J. **2019**, *25*, 2927–2934. doi:10.1002/chem.201803413.
(61) Tsoureas, N.; Mansikkamäki, A.; Layfield, R. A., ChemComm **2020**, *56*, 944–947.
(62) Guo, F.-S.; Tsoureas, N.; Huang, G.-Z.; Tong, M.-L.; Mansikkamäki, A.; Layfield, R. A., Angew. Chem. Int. Ed. **2020**, *59*, 2299–2303. doi:10.1002/anie.201912663.
(63) Kelley, M. P.; Popov, I. A.; Jung, J.; Batista, E. R.; Yang, P., Nat. Commun. **2020**, *11*, 1558. doi:10.1038/s41467-020-15197-w.
(64) Chandrasekar, A.; Joshi, M.; Ghanty, T. K., J. Chem. Sci. **2019**, *131*, 122.1–122.11. doi:10.1007/s12039-019-1713-7.
(65) Biedermann, F.; Schneider, H.-J., Chem. Rev. **2016**, *116*, 5216–5300. doi:10.1021/acs.chemrev.5b00583.
(66) Luo, Y.-R., *Comprehensive Handbook of Chemical Bond Energies*; CRC Press: Boca Raton, **2017**.
(67) Luo, Y.-R., *Handbook of Bond Dissociation Energies in Organic Compounds*; CRC Press: Boca Raton, **2002**. doi:10.1201/9781420039863.
(68) Ma, Q.; Werner, H.-J., J. Chem. Theory Comput. **2019**, *15*, 1044–1052. doi:10.1021/acs.jctc.8b01098.
(69) Waller, M.; Grimme, S.In *Handbook of Computational Chemistry*; J., Leszczynski, A., Kaczmarek-Kedziera, T. G., Puzyn, M., Papadopoulos, R. K. Heribert, M., Shukla, Ed.; Springer International Publishing: New York, **2017**; pp. 593–619. doi:10.1007/978-3-319-27282-5_12.
(70) Rezac, J.; Riley, K. E.; Hobza, P., J. Chem. Theory Comput. **2011**, *7*, 2427–2438. doi:10.1021/ct2002946.
(71) Jurecka, P.; Sponer, J.; Cerny, J.; Hobza, P., Phys. Chem. Chem. Phys. **2006**, *8*, 198–1993. doi:10.1039/B600027D.
(72) Takatani, T.; Hohenstein, E.; Malagoli, M.; Marshall, M.; Sherrill, C., J. Phys. Chem. **2011**, *135*, 194102.
(73) Dral, P.; Wu, X.; Thiel, W., J. Chem. Theory Comput. **2019**, *15*, 1743–1760. doi:10.1021/acs.jctc.8b01265.
(74) Cremer, D.; Kraka, E., Curr. Org. Chem. **2010**, *14*, 1524–1560. doi:10.2174/138527210793563233.
(75) Andrés, J.; Ayers, P. W.; Boto, R. A.; Carbó-Dorca, R.; Chermette, H.; Cioslowski, J.; Contreras-García, J.; Cooper, D. L.; Frenking, G.; Gatti, C.; et al. J. Comput. Chem. **2019**, *40*, 2248–2283. doi:10.1002/jcc.26003.
(76) Kaupp, M.; Danovich, D.; Shaik, S., Coord. Chem. Rev. **2017**, *344*, 355–362. doi:10.1016/j.ccr.2017.03.002.
(77) Zhao, L.; von Hopffgarten, M.; Andrada, D. M.; Frenking, G., WIREs Comput. Mol. Sci. **2018**, *8*, 1–37.
(78) Stasyuk, O. A.; Sedlak, R.; Guerra, C. F.; Hobza, P., J. Chem. Theory Comput. **2018**, *14*, 3440–3450. doi:10.1021/acs.jctc.8b00034.
(79) Levine, D. S.; Head-Gordon, M., Proc. Natl. Acad. Sci. U.S.A. **2017**, *114*, 12649–12656. doi:10.1073/pnas.1715763114.
(80) Lao, K. U.; Herbert, J. M., J. Chem. Theory Comput. **2016**, *12*, 2569–2582. doi:10.1021/acs.jctc.6b00155.
(81) Kilpatrick, A. F. R.; Green, J. C.; Cloke, F. G. N., Organometallics **2010**, *34*, 4830–4843. doi:10.1021/acs.organomet.5b00363.
(82) Goodman, H.; Mei, L.; Gianetti, T. L., Front. Chem. **2019**, *7*, 365.1–19. doi:10.3389/fchem.2019.00365.
(83) Zhao, L.; Zhi, M.; Frenking, G., Int. J. Quantum Chem. **2022**, *122*, e26773.
(84) Wilson, E. B.; Decius, J. C.; Cross, P. C.; *Molecular Vibrations*; McGraw-Hill: New York, **1955**.
(85) Woodward, L. A., *Introduction to the Theory of Molecular Vibrations and Vibrational Spectroscopy*; Oxford University Press: Oxford, **1972**.
(86) Herzberg, G., *Molecular Spectra and Molecular Structure*. Vol. *I*: 2nd ed; Reitell Press: New York, **2008**.
(87) Herzberg, G., *Molecular Spectra and Molecular Structure. Volume II: Infrared and Raman Spectra of Polyatomic Molecules*; Krieger Publishing Co: New York, **1991**.
(88) Herzberg, G.; Huber, K. P., *Molecular Spectra and Molecular Structure. IV. Constants of Diatomic Molecules*; Van Nostrand, Reinhold: New York, **1979**.
(89) Califano, S., *Vibrational States*; Wiley: New York, **1976**.
(90) Meier, R. J., Vib. Spectrosc. **2007**, *43*, 26–37. doi:10.1016/j.vibspec.2006.06.003.
(91) Konkoli, Z.; Cremer, D., Int. J. Quantum Chem. **1998**, *67*, 1–9. doi:10.1002/(SICI)1097-461X(1998)67:1⟨1::AID-QUA1⟩3.0.CO;2-Z.
(92) Konkoli, Z.; Larsson, J. A.; Cremer, D., Int. J. Quantum Chem. **1998**, *67*, 11–27. doi:10.1002/(SICI)1097-461X(1998)67:1⟨11::AID-QUA2⟩3.0.CO;2-1.
(93) Konkoli, Z.; Cremer, D., Int. J. Quantum Chem. **1998**, *67*, 29–40. doi:10.1002/(SICI)1097-461X(1998)67:1⟨29::AID-QUA3⟩3.0.CO;2-0.
(94) Konkoli, Z.; Larsson, J. A.; Cremer, D., Int. J. Quantum Chem. **1998**, *67*, 41–55. doi:10.1002/(SICI)1097-461X(1998)67:1⟨41::AID-QUA4⟩3.0.CO;2-Z.
(95) Cremer, D.; Larsson, J. A.; Kraka, E. In *Theoretical and Computational Chemistry*; C., Parkanyi, Ed.; Elsevier: Amsterdam, **1998**; pp. 259–327. doi:10.1016/S1380-7323(98)80012-5.
(96) Mishra, B. K.; Sathyamurthy, N., J. Chem. Phys. **2007**, *111*, 2139–2147. doi:10.1021/jp065584r.
(97) Mishra, B. K.; Karthikeyan, S.; Ramanathan, V., J. Chem. Theory Comput. **2012**, *8*, 1935–1942. doi:10.1021/ct300100h.
(98) Dinadayalane, T. C.; Paytakov, G.; Leszczynski, J., J. Mol. Model. **2013**, *19*, 2855–2864. doi:10.1007/s00894-012-1729-0.
(99) Rahnamaye Aliabad, H. A.; Chahkandi, M., Z. Anorg. Allg. Chem. **2017**, *643*, 420–431. doi:10.1002/zaac.201600423.
(100) Flower, K. R.; Hitchcock, P. B., J. Organomet. Chem. **1996**, *507*, 275–277. doi:10.1016/0022-328X(95)05747-D.
(101) Costabile, C.; Milano, G.; Cavallo, L.; Guerra, G., Macromolecules **2001**, *34*, 7952–7960. doi:10.1021/ma010673h.
(102) Ernst, R. D., Chem. Rev. **1988**, *88*, 1255–1291. doi:10.1021/cr00089a013.
(103) Prohens, R.; Sande, D.; Font-Bardia, M.; Franconetti, A.; Gonzalez, J. F.; Frontera, A., Cryst. Growth Des. **2019**, *19*, 3989–3997. doi:10.1021/acs.cgd.9b00387.
(104) Kraka, E.; Zou, W.; Tao, Y., WIREs Comput. Mol. Sci. **2020**, *10*, 1480. doi:10.1002/wcms.1480.
(105) Zou, W.; Izotov, D.; Cremer, D., J. Phys. Chem. A **2011**, *115*, 8731–8742. doi:10.1021/jp2041907.
(106) Zou, W.; Filatov, M.; Cremer, D., Int. J. Quantum Chem. **2012**, *112*, 3277–3288. doi:10.1002/qua.24116.
(107) Zou, W.; Cremer, D., Aust. J. Chem. **2014**, *67*, 435. doi:10.1071/CH13480.
(108) Cremer, D.; Pople, J. A., J. Am. Chem. Soc. **1975**, *97*, 1354–1358. doi:10.1021/ja00839a011.
(109) Zou, W.; Kalescky, R.; Kraka, E.; Cremer, D., J. Chem. Phys. **2012**, *137*, 084114. doi:10.1063/1.4747339.

Can. J. Chem. Downloaded from cdnsciencepub.com by University of Alberta on 09/01/23
For personal use only.

(110) Zou, W.; Kalescky, R.; Kraka, E.; Cremer, D., J. Mol. Model. **2012**, *19*, 2865–2877. doi:10.1007/s00894-012-1697-4.
(111) Barone, V.; Alessandrini, S.; Biczysko, M.; Cheeseman, J. R.; Clary, D. C.; McCoy, A. B.; DiRisio, R. J.; Neese, F.; Melosso, M.; Puzzarini, C., Nat. Rev. Methods Primers **2021**, *1*, 38. doi:10.1038/s43586-021-00034-1.
(112) Baiz, C. R.; Błasiak, B.; Bredenbeck, J.; Cho, M.; Choi, J.-H.; Corcelli, S. A.; Dijkstra, A. G.; Feng, C.-J.; Garrett-Roe, S.; Ge, N.-H.; et al., Chem. Rev. **2020**, *120*, 7152–7218. doi:10.1021/acs.chemrev.9b00813.
(113) Beć, K. B.; Grabska, J.; Huck, C. W., Spectrochim. Acta A Mol. Biomol. Spectrosc. **2021**, *254*, 1–11. doi:10.1016/j.saa.2021.119625.
(114) Hess, C., Chem. Soc. Rev. **2021**, *50*, 3519–3564. doi:10.1039/D0CS01059F.
(115) Cassabaum, A. A.; Bera, K.; Rich, C. C.; Nebgen, B. R.; Kwang, S. Y.; Clapham, M. L.; Frontiera, R. R., J. Chem. Phys. **2020**, *153*, 030901. doi:10.1063/5.0009976.
(116) Graefe, C. T.; Punihaole, D.; Lynch, M. J.; Silva, W. R.; Frontiera, R. R., J. Raman Spectrosc. **2021**, *52*, 404–411. doi:10.1002/jrs.5970.
(117) Graefe, C. T.; Punihaole, D.; Harris, C. M.; Lynch, M. J.; Leighton, R.; Frontiera, R. R., Anal. Chem. **2019**, *91*, 8723–8731. doi:10.1021/acs.analchem.9b01731.
(118) Beć, K. B.; Huck, C. W., Front. Chem. **2019**, *7*, 2296–2646. doi:10.3389/fchem.2019.00048.
(119) Markelz, A. G.; Mittleman, D. M., ACS Photonics **2022**, *9*, 1117–1126. doi:10.1021/acsphotonics.2c00228.
(120) Whaley-Mayda, L.; Guha, A.; Penwell, S. B.; Tokmakoff, A., J. Am. Chem. Soc. **2021**, *143*, 3060–3064. doi:10.1021/jacs.1c00542.
(121) Wilson, E. B., J. Chem. Phys. **1941**, *9*, 76–84. doi:10.1063/1.1750829.
(122) Decius, J., J. Chem. Phys. **1963**, *38*, 241–248. doi:10.1063/1.1733469.
(123) Zou, W.; Cremer, D., Theor. Chem. Acc. **2014**, *133*, 1451–1466. doi:10.1007/s00214-014-1451-3.
(124) Kalescky, R.; Kraka, E.; Cremer, D., Mol. Phys. **2013**, *111*, 1497–1510. doi:10.1080/00268976.2013.796070.
(125) Kalescky, R.; Kraka, E.; Cremer, D., Inorg. Chem. **2013**, *53*, 478–495. doi:10.1021/ic4024663.
(126) Verma, N.; Tao, Y.; Zou, W.; Chen, X.; Chen, X.; Freindorf, M.; Kraka, E., Sensors **2020**, *20*, 2358. doi:10.3390/s20082358.
(127) Delgado, A. A. A.; Humason, A.; Kalescky, R.; Freindorf, M.; Kraka, E., Molecules **2021**, *26*, 950–1-950-25. doi:10.3390/molecules26040950.
(128) Oliveira, V. P.; Marcial, B. L.; Machado, F. B.; Kraka, E., ChemPlusChem **2021**, *86*, 1199–1210. doi:10.1002/cplu.202100285.
(129) Delgado, A. A. A.; Sethio, D.; Munar, I.; Aviyente, V.; Kraka, E., J. Chem. Phys. **2020**, *153*, 224303–1-224303-11. doi:10.1063/5.0034765.
(130) Freindorf, M.; Kraka, E., J. Mol. Model. **2020**, *26*, 281–1-281-15. doi:10.1007/s00894-020-04519-w.
(131) Kraka, E.; Freindorf, M. In *Topics in Organometallic Chemistry - New Directions in the Modeling of Organometallic Reactions*; A., Lledós; G., Ujaque, Ed.; Springer: Berlin, Heidelberg, **2020**; Vol. *67*; pp. 1–43. doi:10.1007/3418_2020_57.
(132) McCutcheon, M.; Freindorf, M.; Kraka, E., J. Chem. Phys. **2022**, *157*, 014301. doi:10.1063/5.0094567.
(133) Tao, Y.; Zou, W.; Sethio, D.; Verma, N.; Qiu, Y.; Tian, C.; Cremer, D.; Kraka, E., J. Chem. Theory Comput. **2019**, *15*, 1761–1776. doi:10.1021/acs.jctc.8b01279.
(134) Nanayakkara, S.; Tao, Y.; Kraka, E., J. Chem. Theory Comput. **2022**, *18*, 562–579. doi:10.1021/acs.jctc.1c00357.
(135) Szalay, V., J. Chem. Phys. **2014**, *140*, 234107. doi:10.1063/1.4883195.
(136) Likura, H.; Tsuneda, T.; Yanai, T.; Hirao, K., J. Chem. Phys. **2001**, *115*, 3540–3544. doi:10.1063/1.1383587.
(137) Grimme, S.; Ehrlich, S.; Goerigk, L., J. Comp. Chem. **2011**, *32*, 1456–1465. doi:10.1002/jcc.21759.
(138) Weigend, F., Phys. Chem. Chem. Phys. **2006**, *8*, 1057–1065. doi:10.1039/b515623h.
(139) Choi, T. H.; Young-Kyu, H., Bull. Korean Chem. Soc. **2011**, *32*, 4195–4198. doi:10.5012/bkcs.2011.32.12.4195.
(140) Grimme, S.; Neese, F., J. Chem. Phys. **2007**, *127*, 154116. doi:10.1063/1.2772854.
(141) Grimme, S.; Antony, J.; Ehrlich, S.; Krieg, H., J. Chem. Phys. **2010**, *132*, 154104. doi:10.1063/1.3382344.
(142) Kaiser, K.; Scriven, L. M.; Schulz, F.; Gawel, P.; Gross, L.; Anderson, H. L., Science **2019**, *365*, 1299–1301. doi:10.1126/science.aay1914.
(143) Zou, W.; Tao, Y.; Cremer, D.; Kraka, E., J. Chem. Phys. **2020**, *152*, 154107. doi:10.1063/1.5144278.
(144) Bader, R. F. W., Atoms in molecules: a quantum theory. In *International Series of Monographs on Chemistry*; Oxford University Press: USA, **1990**.
(145) Bader, R., A quantum theory of molecular structure and its applications. In *Encyclopedia of Computational Chemistry*; P. v., Schleyer, Ed.; John Wiley and Sons: Chichester, U.K., **1998**, Vol. *1*, pp. 64–86.
(146) Cremer, D.; Kraka, E., Angew. Chem. Int. Ed. **1984**, *23*, 627–628. doi:10.1002/anie.198406271.
(147) Cremer, D.; Kraka, E., Croatica Chem. Acta **1984**, *57*, 1259–1281.
(148) Cremer, D., *Modelling of Structure and Properties of Molecules*; Z. B., Maksic, Ed.; Horwood Ellis: Chichester, **1987**; p 125.
(149) Sethio, D.; Oliveira, V.; Kraka, E., Molecules **2018**, *23*, 2763. doi:10.3390/molecules23112763.
(150) Wick, C. R.; Clark, T., J. Mol. Model. **2018**, *24*, 142. doi:10.1007/s00894-018-3684-x.
(151) Wick, C. R.; Clark, T., Crystals **2017**, *7*, 43.
(152) Jablonski, M., ChemistryOpen **2019**, *8*, 497–507.
(153) Jablonski, M., J. Comput. Chem. **2018**, *39*, 2183–2195.
(154) Shahbazian, S., Chem. Eur. J. **2018**, *24*, 5401–5405. doi:10.1002/chem.201705163.
(155) Bader, R. F. W., J. Phys. Chem. A **2009**, *113*, 1039–10396.
(156) Kalescky, R.; Kraka, E.; Cremer, D., J. Phys. Chem. A **2013**, *118*, 223–237. doi:10.1021/jp4092514.
(157) Grimme, S.; Mück-Lichtenfeld, C.; Erker, G.; Kehr, G.; Wang, H.; Beckers, H.; Wilners, H., Angew. Chem. Int. Ed. **2009**, *48*, 2592–2595. doi:10.1002/anie.200805751.
(158) Matta, C.; Hernandez-Trujillo, J.; Tang, T.-H.; Bader, R., Chem. Eur. J. **2009**, *9*, 1940–1951. doi:10.1002/chem.200204626.
(159) Politzer, P.; Murray, J. S., ChemPhysChem **2020**, *21*, 579–588. doi:10.1002/cphc.201900968.
(160) Fabrizio, A.; Grisafi, A.; Meyer, B.; Ceriotti, M.; Corminboeuf, C., Chem. Sci. **2019**, *10*, 9424–9432. doi:10.1039/C9SC02696G.
(161) Møller, C.; Plesset, M. S., Phys. Rev. **1934**, *46*, 618–622. doi:10.1103/PhysRev.46.618.
(162) McLean, A. D.; Chandler, G. S., J. Chem. Phys. **1980**, *72*, 5639–5648. doi:10.1063/1.438980.
(163) Godfrey-Kittle, A.; Cafiero, M., Int. J. Quantum Chem. **2006**, *106*, 2035–2043. doi:10.1002/qua.20969.
(164) Jorge, F. E.; Canal Neto, A.; Camiletti, G. G.; Machado, S. F., J. Chem. Phys. **2009**, *130*, 064108. doi:10.1063/1.3072360.
(165) Canal-Neto, A.; Muniz, E. P.; Centoducatte, R.; Jorge, F. E., J. Mol. Struct. Theochem. **2005**, *718*, 219–224.
(166) Zhao, Y.; Truhlar, D. G., Theor. Chem. Acc. **2008**, *120*, 215–241. doi:10.1007/s00214-007-0310-x.
(167) Dyall, K. G., J. Chem. Phys. **1997**, *106*, 9618–9626. doi:10.1063/1.473860.
(168) Dyall, K. G., J. Comput. Chem. **2002**, *23*, 786–793. doi:10.1002/jcc.10048.
(169) Filatov, M.; Zou, W.; Cremer, D., J. Chem. Phys. A **2012**, *116*, 3481–3486. doi:10.1021/jp301224u.
(170) Filatov, M.; Zou, W.; Cremer, D., J. Chem. Theory Comput. **2012**, *8*, 875–882. doi:10.1021/ct2008632.
(171) Filatov, M.; Zou, W.; Cremer, D., J. Chem. Phys. **2012**, *137*, 054113. doi:10.1063/1.4742175.
(172) Zou, W.; Filatov, M.; Cremer, D., J. Chem. Phys. **2012**, *137*, 084108. doi:10.1063/1.4747335.
(173) Filatov, M.; Zou, W.; Cremer, D., J. Chem. Phys. **2012**, *137*, 131102. doi:10.1063/1.4757568.
(174) Yoshizawa, T.; Zou, W.; Cremer, D., J. Chem. Phys. **2016**, *145*, 184104. doi:10.1063/1.4964765.
(175) Yoshizawa, T.; Zou, W.; Cremer, D., J. Chem. Phys. **2017**, *146*, 134109. doi:10.1063/1.4979499.
(176) Yoshizawa, T.; Filatov, M.; Cremer, D.; Zou, W., Mol. Phys. **2019**, *117*, 1164–1171. doi:10.1080/00268976.2018.1530463.
(177) Zou, W.; Filatov, M.; Cremer, D., J. Chem. Phys. **2011**, *134*, 244117. doi:10.1063/1.3603454.
(178) Zou, W.; Filatov, M.; Cremer, D., J. Chem. Phys. **2015**, *142*, 214106. doi:10.1063/1.4921915.

(179) Zou, W.; Filatov, M.; Cremer, D., J. Chem. Theory Comput. **2012**, *8*, 2617–2629. doi:10.1021/ct300127e.
(180) Ditchfield, R.; Hehre, W. J.; Pople, J. A., J. Chem. Phys. **1971**, *54*, 724–728. doi:10.1063/1.1674902.
(181) Becke, A. D., Phys. Rev. A **1988**, *38*, 3098–3100. doi:10.1103/PhysRevA.38.3098.
(182) Goerigk, L.; Grimme, S., J. Chem. Theory Comput. **2011**, *7*, 291–309. doi:10.1021/ct100466k.
(183) Dunning, T. H., J. Chem. Phys. **1989**, *90*, 1007–1023. doi:10.1063/1.456153.
(184) Woon, D. E.; Dunning, T. H., J. Chem. Phys. **1993**, *98*, 1358–1371. doi:10.1063/1.464303.
(185) Balabanov, N. B.; Peterson, K. A., J. Chem. Phys. **2005**, *123*, 064107. doi:10.1063/1.1998907.
(186) Toma, M.; Kuvek, T.; Vrček, V., J. Phys. Chem. A **2020**, *124*, 8029–8039. doi:10.1021/acs.jpca.0c06663.
(187) Perdew, J. P.; Burke, K.; Ernzerhof, M., Phys. Rev. Lett. **1996**, *77*, 3865–3868. doi:10.1103/PhysRevLett.77.3865.
(188) Perdew, J. P.; Ernzerhof, M.; Burke, K., J. Chem. Phys. **1996**, *105*, 9982–9985. doi:10.1063/1.472933.
(189) Rappoport, D.; Furche, F., J. Chem. Phys. **2010**, *133*, 134105. doi:10.1063/1.3484283.
(190) Weigend, F.; Ahlrichs, R., Phys. Chem. Chem. Phys. **2005**, *7*, 3297–3305. doi:10.1039/b508541a.
(191) Frisch, M. J.; Trucks, G. W.; Schlegel, H. B.; Scuseria, G. E.; Robb, M. A.; Cheeseman, J. R.; Scalmani, G.; Barone, V.; Petersson, G. A.; Nakatsuji, H.; et al., *Gaussian 16*; Gaussian, Inc.: Wallingford, CT, **2016**.
(192) Kraka, E.; Zou, W.; Filatov, M.; Gräfenstein, J.; Izotov, D.; Gauss, J.; He, Y.; Wu, A.; Konkoli, Z.; Polo, V.; et al., COLOGNE201919; Dallas, Texas, **2019**.
(193) Zou, W.; Tao, Y.; Freindorf, M.; Makoś, M. Z.; Verma, N.; Cremer, D.; Kraka, E. *Local Vibrational Mode Analysis (LModeA). Computational and Theoretical Chemistry Group (CATCO)*; Southern Methodist University: Dallas, TX, USA, **2022**.
(194) Bader, R. F. W., Chem. Rev. **1991**, *91*, 893–928. doi:10.1021/cr00005a013.
(195) Bader, R. F. W., Monatsh. Chemie **2005**, *136*, 819–854. doi:10.1007/s00706-005-0307-x.
(196) Keith, T. A. AIMALL. TK Gristmill Software: Overland Park KS **2017**.
(197) Kraka, E.; Setiawan, D.; Cremer, D., J. Comput. Chem. **2015**, *37*, 130–142. doi:10.1002/jcc.24207.
(198) Kraka, E.; Cremer, D., Rev. Proc. Quim. **2012**, 39–42.
(199) Setiawan, D.; Kraka, E.; Cremer, D., J. Phys. Chem. A **2015**, *119*, 9541–9556. doi:10.1021/acs.jpca.5b05157.
(200) Luo, Y.-R., *Comprehensive Handbook of Chemical Bond Energies*; Taylor and Francis: Boca Raton, FL, **2007**.
(201) Moltved, K. A.; Kepp, K. P., J. Chem. Theory Comput. **2018**, *14*, 3479–3492. doi:10.1021/acs.jctc.8b00143.
(202) Morse, M. D., Acc. Chem. Res. **2018**, *52*, 119–126. doi:10.1021/acs.accounts.8b00526.
(203) Kalescky, R.; Kraka, E.; Cremer, D., Int. J. Quantum Chem. **2014**, *114*, 1060–1072. doi:10.1002/qua.24626.
(204) Kalescky, R.; Zou, W.; Kraka, E.; Cremer, D., J. Phys. Chem. A **2014**, *118*, 1948–1963. doi:10.1021/jp4120628.
(205) Oliveira, V.; Kraka, E.; Cremer, D., Inorg. Chem. **2016**, *56*, 488–502. doi:10.1021/acs.inorgchem.6b02358.
(206) Setiawan, D.; Sethio, D.; Cremer, D.; Kraka, E., Phys. Chem. Chem. Phys. **2018**, *20*, 23913–23927. doi:10.1039/C8CP03843K.
(207) Swart, M., Inorganica Chim. Acta **2007**, *360*, 179–189. doi:10.1016/j.ica.2006.07.073.
(208) Haaland, A., J. Am. Chem. Soc. **1979**, *12*, 416–22.
(209) Dowben, P. A.; Driscoll, D. C.; Tate, R. S.; Boag, N. M., Organometallics **1988**, *7*, 305–308. doi:10.1021/om00092a011.
(210) Zhang, G.; Zhang, H.; Sun, M.; Liu, Y.; Pang, X.; Yu, X.; Liu, B.; Li, Z., J. Comput. Chem. **2007**, *28*, 2260–2274. doi:10.1002/jcc.20629.
(211) Lefebvre, C.; Rubez, G.; Khartabil, H.; Boisson, J.-C.; Contreras-García, J.; Hénon, E., Phys. Chem. Chem. Phys. **2017**, *19*, 17928–17936. doi:10.1039/C7CP02110K.
(212) Zierkiewicz, W.; Michalczyk, M.; Scheiner, S., Molecules **2021**, *26*, 1740. doi:10.3390/molecules26061740.
(213) Politzer, P.; Murray, J. S., J. Comput. Chem. **2018**, *39*, 464–471. doi:10.1002/jcc.24891.
(214) Gadre, S. R.; Suresh, C. H.; Mohan, N., Molecules **2021**, *26*, 3289.
(215) Politzer, P.; Murray, J. S., ChemPhysChem **2020**, *21*, 579–588. doi:10.1002/cphc.201900968.

Can. J. Chem. Downloaded from cdnsciencepub.com by University of Alberta on 09/01/23
For personal use only.